

AUS Repository

Carbon Dots-Based Polymer Composites for Conductive Electrodes

Item Type	Thesis
Authors	Ali, Amaal Abdulraheb
Download date	2026-04-15 10:33:18
Link to Item	http://hdl.handle.net/11073/25377

CARBON DOTS-BASED POLYMER COMPOSITES FOR CONDUCTIVE
ELECTRODES

by
Amaal Abdulraqeb Ali

A Thesis presented to the Faculty of the
American University of Sharjah
College of Engineering
In Partial Fulfilment
of the Requirements
for the Degree of

Master of Science in
Biomedical Engineering

Sharjah, United Arab Emirates

April 2023

Declaration of Authorship

I declare that this thesis is my own work and, to the best of my knowledge and belief, it does not contain material published or written by a third party, except where permission has been obtained and/or appropriately cited through full and accurate referencing.

SignatureAmaal Abdulraqeb Ali.....

Date.....13-April-2023.....

The Author controls copyright for this report.
Material should not be reused without the consent of the author. Due
acknowledgement should be made where appropriate.

© Year 2023

Amaal Abdulraqeb Ali

ALL RIGHTS RESERVED

Approvals

We, the undersigned, approve the Masters Thesis written by:
Amaal Abdulraqeb Ali

Thesis Title: Carbon Dots-Based Polymer Composites for
Conductive Electrodes

Date of Defense: 13.April.2023

Name, Title and Affiliation

Signature

Dr. Mohammad H. Al-Sayah
Professor/Associate Professor/Assistant Professor
Department of Biology, Chemistry and Environmental
Sciences
Thesis Advisor

Dr. Amani Al-Othman
Associate Professor
Department of Chemical and Biological Engineering
Thesis Co-advisor

Dr. Hasan Al-Nashash
Professor
Department of Electrical Engineering
Thesis Co-advisor

Dr. Rana Sabouni
Associate Professor
Department of Chemical and Biological Engineering
Thesis Examiner (Internal)

Dr. Paul Nancarrow
Professor
Department of Chemical and Biological Engineering
Thesis Examiner (Internal)

Accepted by:
Dr. Fadi Aloul
Dean
College of Engineering

Dr. Mohamed Al-Tarhuni
Vice Provost for Research and Graduate Studies
Office of Research and Graduate Studies

Acknowledgements

First and foremost, I am grateful to Allah, the All-Knowing, for giving me the ability to complete this work, for without His guidance, none of this would have been possible.

I would like to express my sincere appreciation to my research advisors, Dr. Mohammad Al-Sayah, Dr. Amani Al-Othman, and Dr. Hasan Al-Nashash who not only guided me throughout this project but were also an enormous source of motivation for me during my two years at AUS. I have learned a lot under their supervision, and for that I am grateful.

I am also extremely thankful to my colleagues and friends Rouba Al-Bostami, Lamis Abdul Kader, Yara Badr, and Heba Abed for supporting me on an academic and personal level and making my stay at AUS feel like home.

I would like to thank the professors of the Biomedical Engineering department who taught me the master level courses with mighty teaching methods and skills. I really appreciate their dignified advice and motivation. I would also like to thank my thesis committee members, Dr. Rana Sabouni and Dr. Paul Nancarrow, who revised this thesis and provided me with valuable feedback to further improve this work.

I am grateful to the Office of Research and Graduate Studies for providing me with the GRA scholarship throughout the master's program. This work added to my experience and knowledge throughout my stay at the university.

Moreover, I would like to thank the “3rd Forum for Women in Research (QUWA): Women Empowerment for Global Impact at University of Sharjah” for supporting this project with a 10,000 AED grant and Abu Dhabi National Oil Company (ADNOC), Emirates NBD and Sharjah Electricity Water & Gas Authority (SEWA), Dubai Electricity and Water Authority R & D Center as the sponsors of QUWA.

Dedication

*To my parents, my role models,
whose endless support, love, and encouragement
have always been my source of strength
in everything I do.*

This work, like everything else I ever do, is dedicated to them.

Abstract

Flexible electrodes have become a topic of interest for implantable applications such as stimulation of muscles atrophying due to nerve damage. Implantable electrodes used for signal recording and/or signal stimulation are composed of metals and metal alloys to benefit from metal's high conductivity, corrosion resistance, and stability. However, due to their inherent rigidity, metal electrodes are limited by their mechanical mismatch with the soft biological tissues. Therefore, flexible alternatives are needed to replace metal electrodes. Several conductive and flexible polymers have been explored to replace metal composites. However, polymer-based composites still possess limitations including high rigidity or toxicity issues. This study presents flexible electrodes based on the highly elastic polymer polydimethylsiloxane (PDMS) and the conductive dopant boronic acid-modified carbon dots (BA-CDs). The potential of the composites as flexible electrodes was evaluated based on their: 1) electrochemical properties (conductivity, bulk resistance, impedance at 1 kHz, charge storage capacity (CSC), and electrochemical stability), 2) elasticity (Young's modulus), 3) biocompatibility, 4) stability in body-like environment and 5) ability to record electrophysiological signals. The developed electrodes composed of 10% BA-CDs and 74% PDMS with 16% glycerol (dispersant) showed a promising conductivity of $9.62 \pm 3.45 \times 10^{-3}$ S/cm, bulk resistance 0.058 ± 0.0135 k Ω , impedance at 1 kHz of 0.964 ± 0.361 M Ω , and a CSC of 21.4 ± 5.9 μ C/cm². Mechanically, the electrodes had a flexibility of 0.0505 ± 0.0218 MPa that is compatible with biological tissues. Post-incubation in phosphate buffer saline (body-like environment), the electrodes performance improved electrochemically but deteriorated mechanically (0.1562 ± 0.0274 MPa) although to a degree still compatible with biological tissues. As surface electrodes, the electrodes recorded heart activity (electrocardiography) and muscle activity (electromyography) with a signal quality comparable to that of the commercial Ag/AgCl electrodes. In terms of biocompatibility, the electrodes showed some toxicity toward cells *in vitro*. However, future dose-response experiments using the conventional fibroblast L929 cells need to yet be conducted to obtain a more accurate understanding of the toxicity of the material.

Search Terms: polydimethylsiloxane (PDMS); boronic acid-modified carbon dots; implantable electrodes; Young's modulus.

Table of Contents

Abstract.....	5
List of Figures	8
List of Tables	12
List of Abbreviations and Symbols.....	13
Chapter 2. Introduction	15
1.1 Background.....	15
1.2 Thesis Objectives	19
1.3 Hypothesis.....	19
1.4 Report Organization.....	20
Chapter 2. Literature review	21
2.1 Peripheral Nerve Injuries	21
2.2 Flexible Implantable Electrodes	22
2.4 Electrically Conductive Boronic Acid-Modified Carbon Dots as Potential PDMS Fillers	28
Chapter 3. Methodology	31
3.1 Experimental protocols	31
3.1.1. Boronic acid-modified carbon dots (BA-CD) synthesis.....	31
3.1.2. BA-CD characterization.....	31
3.1.3. Lab-scale electrode fabrication.....	34
3.1.4. Electrochemical testing.....	36
3.1.5. Mechanical testing.....	41
3.1.6. Stability testing.....	41
3.1.7. Statistical methods.....	42
3.1.8. Biocompatibility testing.....	42
3.1.9. Electrocardiography (ECG) and electromyography (EMG).....	43
Chapter 4. Results and Discussion.....	46
4.1 Overview	46
4.2 BA-CD Characterization.....	46
4.2.1 ATR-IR spectroscopy	46
4.2.2 UV-Vis (absorption) and fluorescence (emission) spectroscopy.....	47

4.2.3	SEM	48
4.2.4	Electrochemical testing: EIS and CV	49
4.3	BA-CD/PDMS Composites: Characterization.....	50
4.3.1	ATR-IR and SEM:	50
4.3.2	Electrochemical testing: EIS and CV	52
4.3.3	Mechanical testing: tensile testing	60
4.3.4	Stability testing: PBS immersion	62
4.4	BA-CD/PDMS Electrode Biocompatibility Testing.....	65
4.5	Electrophysiological Signal Recording: ECG and EMG.....	66
Chapter 5. Conclusion and Future work		70
References.....		72
Appendix A.....		81
Vita.....		83

List of Figures

Figure 1.1 BA-CDs entrapped within pores of the crosslinked polymer chains (PDMS)	18
Figure 2.1 Electron-hole movement. As voltage is applied, the hole shifts towards the negative terminal while the electron moves toward the positive terminal. As the electrons move to accommodate the hole, the location of the holes shifts in the opposite direction. The movement of electrons/holes contributes to the current flow.	29
Figure 3.1 IR spectroscopy theory. When exposed to photons in the IR range, the molecule's different bonds absorb some of the photons to undergo molecular vibrational transitions. The absorbed photons translate into fingerprint peaks that represent different functional groups on the IR spectrum.....	32
Figure 3.2 UV-vis spectroscopy theory. When exposed to photons in the UV-Vis range, the molecule's electrons absorb the photons to undergo electronic transitions. This photon absorption translates into peaks on the UV-vis spectrum that can be used for material characterization.....	33
Figure 3.3 Fluorescence emission spectroscopy theory. As the molecule absorbs light, its electrons get excited after which they relax emitting fluorescence.....	34
Figure 3.4 a. PDMS/BA-CD electrodes molded in 3D printed casting plates of 1 cm diameter and 1 mm thickness; b. cured electrode samples of 1 cm diameter and 1 mm thickness	35
Figure 3.5 PLA casting molds with fused base; 1 cm diameter; 1 mm thickness	36
Figure 3.6 A typical Nyquist plot of a conductive material showing the charge transfer semi-circle and diffusion (Warburg impedance) line at 45°; W = Warburg; R = bulk resistance; R_{ct} = charge transfer resistance	37
Figure 3.7 Vector representation of the impedance complex number; Z' = real impedance; Z'' = imaginary impedance	37
Figure 3.8 Potentiostat used for EIS studies (SP-200, Biologic).....	39
Figure 3.9 PDMS/BA-CD electrode placed in potentiostat vessel	39

Figure 3.10 (a) typical duck shaped and (b) multiple duck shaped CV graphs	40
Figure 3.11 Stress-strain curve for a material loaded till failure	41
Figure 3.12 MTT assay procedure	43
Figure 3.13 (a) BA-CD/PDMS and the (b) Ag/AgCl electrodes used for ECG and EMG measurements.	43
Figure 3.14 Schematic representation of the procedure used to find the SNR of the BA- CD/PDMS and the Ag/AgCl electrodes.	44
Figure 3.15 MATLAB code used to find the SNR of the ECG recorded with the BA- CD electrodes and the Ag/AgCl electrodes.	45
Figure 4.1 ATR-IR spectrum of bare BA-CDs	47
Figure 4.2 UV-vis and fluorescence spectra of bare BA-CDs	48
Figure 4.3 SEM image of bare BA-CDs	48
Figure 4.4 Nyquist plots (with zoomin plots) and cyclic voltammograms of triplicate BA-CD disks of 1 mm thickness	49
Figure 4.5 ATR-IR spectrum of 10% BA-CD, 4% glycerol, and 84% PDMS composites	51
Figure 4.6 SEM image of 10% BA-CD, 16% glycerol, and 74% PDMS composites.	51
Figure 4.7 EDX elemental analysis of 10% BA-CD, 16% glycerol, 74% PDMS composites	52
Figure 4.8 Nyquist plots and cyclic voltammograms of triplicate 10% BA-CD and 90% PDMS composites of 1 mm thickness.....	53
Figure 4.9 Nyquist plots and cyclic voltammograms of triplicate 25% BA-CD and 75% PDMS composites of 1 mm thickness.....	54
Figure 4.10 Nyquist plots and cyclic voltammograms of triplicate 10% BA-CD, 4% glycerol, and 86% PDMS composites of 1 mm thickness	55
Figure 4.11 Nyquist plots and cyclic voltammograms of triplicate 10% BA-CD, 8% glycerol, and 82% PDMS composites of 1 mm thickness	55

Figure 4.12 Nyquist plots and cyclic voltammograms of triplicate 10% BA-CD, 16% glycerol, and 74% PDMS composites of 1 mm thickness	55
Figure 4.13 Nyquist plots and cyclic voltammograms of triplicate 8% glycerol, and 92% PDMS composites of 1 mm thickness.....	56
Figure 4.14 Nyquist plots and cyclic voltammograms of triplicate 16% glycerol, and 84% PDMS composites of 1 mm thickness	56
Figure 4.15 Nyquist plots and cyclic voltammograms of triplicate 10% BA-CD, 16% glycerol, and 74% PDMS composites of 1 mm thickness cured at 60°C....	57
Figure 4.16 Nyquist plots and cyclic voltammograms of triplicate 10% BA-CD, 16% glycerol, and 74% PDMS (9:1) composites of 1 mm thickness.....	58
Figure 4.17 Nyquist plots and cyclic voltammograms of triplicate 10% BA-CD, 16% glycerol, and 74% PDMS (8:1) composites of 1 mm thickness.....	59
Figure 4.18 Elastic region of the tensile stress-strain curve of triplicate 10% BA-CD, 16% glycerol, and 74% PDMS (8:1) electrodes.....	61
Figure 4.19 Triplicate 10% BA-CD, 16% glycerol, and 74% PDMS (8:1) electrodes post-rupture due to applied tensile force	61
Figure 4.20 Average percentage weight change of triplicate 10% BA-CD, 16% glycerol, and 74% PDMS (8:1) electrodes post-immersion in PBS for 7 weeks	63
Figure 4.21 SEM images of 100% PDMS 8:1 (left) and 16% glycerol/84% PDMS 8:1 (right).....	65
Figure 4.22 Viability of cells exposed to bare BA-CDs, bare PDMS (8:1), 16% glycerol/84% PDMS (8:1), and 10% BA-CD/16% glycerol/74% PDMS (8:1) for 48 hours	66
Figure 4.23 ECG measured using 10% BA-CD/16% glycerol/74% PDMS (8:1) and Ag/AgCl electrodes	67
Figure 4.24 EMG measured using 10% BA-CD/16% glycerol/74% PDMS (8:1) and Ag/AgCl electrodes	68

Figure A.1 ECG recording using bare PDMS and PDMS/glycerol when the composite attached to the positive terminal is placed on the left ankle.....82

Figure A.2 Zoomed in portions of the readings obtained with PDMS/Glycerol, Ag/AgCl, and BA-CD/PDMS/Glycerol. High frequency noise is overriding the PDMS/Glycerol signal but lacking in the Ag/AgCl and BA-CD/PDMS/Glycerol ECG82

Figure A.3 EMG recording using PDMS and PDMS/glycerol.....83

List of Tables

Table 2.1 Some implantable electrodes used for tissue stimulation and/or signal recording in the literature	26
Table 4.1 Compositions of the electrodes prepared in this study	50
Table 4.2 Summary of the conductivity, bulk resistance, impedance at 1 kHz, and CSC values for all the prepared and tested compositions.....	59
Table 4.3 Some of the Young's moduli of BA-CD/PDMS electrodes, other flexible polymeric electrodes, and some biological tissues.....	60
Table 4.4 Conductivity, bulk resistance, impedance at 1 kHz, and CSC of the electrodes after PBS immersion for 1 to 12 weeks.....	62

List of Abbreviations and Symbols

A	Area
ATR	Attenuated Total Reflectance
BA-CDs	Boronic Acid-Modified Carbon Dots
CDs	Carbon Dots
CNS	Central Nervous System
CNT	Carbon Nanotubes
CSC	Charge Storage Capacity
CV	Cyclic Voltammetry
DMSO	Dimethyl Sulfoxide
ECG	Electrocardiography
EIS	Electrochemical Impedance Spectroscopy
EMG	Electromyography
FIEs	Flexible Implantable Electrodes
IR	Infrared Spectroscopy
MTT	3-(4,5-dimethylthiazol-2-yl)-2,5-diphenyl tetrazolium bromide
PANI	Polyaniline
PBA	Phenylboronic Acid
PBS	Phosphate Buffer Saline
PDMS	Polydimethylsiloxane
PEDOT-PEG	(3,4-ethylenedioxythiophene)-polyethylene glycol
PEDOT:PSS	(3,4-ethylenedioxythiophene):poly(sodium 4-styrenesulfonate)
PLA	Poly(lactic Acid)
PNIs	Peripheral Nerve Injuries
PNS	Peripheral Nervous System
R	Bulk Resistance
R _{ct}	Charge Transfer Resistance
SEM	Scanning Electron Microscopy
SNR	Signal-to-Noise Ratio
TiO ₂	Titanium Dioxide
UV-vis	Ultraviolet-Visible
W	Warburg impedance

Z'	Real impedance
Z''	Imaginary impedance
Φ	Phase angle

Chapter 1. Introduction

1.1 Background

Activities of the human body are electrically powered by the battery-like performance of cell membranes, thereby, making humans more or less electric machines capable of unique abilities like speech, logic, and special motions [1]. It has long been established that the function of muscles is governed by nerves which are controlled by electricity. Electricity is the only method fast enough to relay the signals needed for human movements, as explained by Luigi Galvani's concept of bioelectricity [2]. Nerves constitute a part of the electrically driven nervous system which, due to its characteristics of conductivity and irritability, perceive and rapidly respond to external and internal stimuli. Therefore, the nervous system maintains body homeostasis and controls voluntary and involuntary human activities such as speaking, breathing, thinking, and walking, among others, making the nervous system involved in nearly every aspect of our well-being [3]. Owing to their importance, malfunctioning of the electrical processes due to a damage in the nervous system could result in some serious disabilities. For instance, peripheral nerves, a network of nerves that connects the central nervous system (brain and spinal cord) to the rest of the body, are highly susceptible to injury due to their fragile nature. Damage to peripheral nerves, known as peripheral nerve injuries (PNIs), can discontinue the transmission of the electrical signal to the target organ/muscle. This can in turn result in serious disabilities such as the irreversible death of the target muscle due to lack of stimulation by a nerve [4].

Combining our understanding of the science of neurology with engineering principles allowed the development of strategies that could possibly combat such disabilities involving nerve damage. Of such advances currently gaining momentum are implantable electrodes [5], [6]. Implantable electrodes serve as an artificial interface between the delicate body tissues and an external device to either electrically stimulate a tissue or measure electrical signals [7], [8]. However, the type of electrode material used presents a challenge due to the strict standards that need to be met to qualify an electrode for direct contact with body tissues especially the fragile nervous tissue. Ideally, an electrode implant should be mechanically compatible to the physiological tissues, possess electrical conductivity with low impedance, resist corrosion, be

biocompatible, and withstand long-term implantation while maintaining the same ability to stimulate tissues and/or record signals [6].

Conventionally, noble metals and metal alloys have been utilized as implantable electrode materials due to their conductivity in physiological media, biocompatibility, and chemical stability. However, metal-based electrodes bring with them several drawbacks including mainly the mechanical mismatch between the harsh metal and the delicate body tissues [5], [7]. Therefore, interest has been recently shifting toward developing flexible conductive electrode materials that could substitute metals. Of the materials explored, polymers have received extensive attention, whether intrinsically conductive polymers or poorly conductive polymers combined with conductive materials that can boost the polymer's conductivity. One particularly interesting polymer in this application is the synthetic polymer polydimethylsiloxane (PDMS). PDMS is defined by its softness, elasticity due to its low Young's modulus, chemical stability, biocompatibility, gas penetrability, inertness in physiological conditions, and low cost [9]–[13]. Importantly, PDMS has been used for long-term implantation and reported to maintain its elasticity and integrity [9], thereby making PDMS an especially suitable material for implantation purposes [14], [15]. Despite its suitable implantation features, PDMS lacks the needed electrical conductivity [16]. To compensate for its non-conductivity, several studies incorporated electrically conductive materials such as carbon nanotubes [17] and zirconium phosphate [18] into PDMS and reported improved electrical performance while maintaining the polymer's elastic features. For instance, Al-Othman et al. [18] studied the use of zirconium phosphate as a conductive PDMS filler and reported improved impedance and conductivity compared to the conventional gold-based electrodes. However, this study did not assess the flexibility of this composite [18]. Another study by Alatom et al. [19] explored the use of the conductive nanosized metal oxide, titanium dioxide (TiO_2), as a commercial silicone filler and reported enhanced conductivity, bulk impedance and electrochemical stability, and an elasticity comparable to that of skin and spinal cord tissues [19]. However, this study did not assess the biocompatibility of the fabricated electrodes. It is worth noting that nano- TiO_2 has been previously reported to be cytotoxic [20]. Therefore, evaluating its biocompatibility *in vitro* is necessary to more accurately evaluate its potential as a filler for future use as an implantable electrode. Although providing promising results, the

work by Al-Othman et al. [18] and Alatoon et al. [19] still involve the use of a rigid metal component and fail to assess the cytocompatibility of the electrodes. Replacing the metal components with a conductive, yet less harsh material that is biocompatible could possibly further improve the elasticity and biocompatibility of the electrodes. Other studies substituted metal-based fillers by using intrinsically conductive polymers with PDMS. Almufleh et al. [21] used the conductive polymer polyaniline (PANI) with commercial silicone and reported similar improved electrical performance in terms of impedance, conductivity and electrochemical stability, and mechanical performance of the electrodes [21]. Despite the improved performance, this work like the other studies discussed did not assess the biocompatibility of the electrodes. PANI is known to possess cytotoxicity which could limit the progress of such PANI-based electrodes *in vitro* and/or *in vivo* [22]. Furthermore, the amount of PANI incorporated in the PDMS is restricted by PANI's semi-flexibility [23] that can hence possibly reduce the elasticity of PDMS. Therefore, there is still a need to replace such fillers with more biocompatible, metal-free ones.

One group of conductive, biocompatible materials that can potentially substitute the toxic metal or polymeric fillers are carbon-based nanomaterials. Carbon-based nanomaterials have been gaining interest for biomedical applications including electrodes due to their favourable properties such as biocompatibility, conductivity, easy surface functionalization and stability, among other properties [24].

Carbon dots (CDs) are one type of fluorescent carbon-based nanomaterials containing functional group-rich surfaces, with sizes typically lower than 10 nm. Due to their abundant possible surface functional groups, CD properties can be further tuned for a particular application by modifying their surface functionality [24]. One possible modification that could enhance CDs electrical conductivity is functionalizing their surface with boronic acid. Boronic acid-modified CDs (BA-CDs) are expected to have superior conductivity compared to bare CDs owing to the presence of Boron. Boron contains holes (empty electron locations) that could shift from one atom to the next with the movement of electrons, thereby permitting the conduction of electricity [25]. Therefore, combining PDMS with BA-CDs, which can be trapped within the PDMS polymeric matrix as shown in Figure 1.1, could possibly provide an electrode

characterized by conductivity and flexibility for future implantable stimulatory and/or sensing applications.

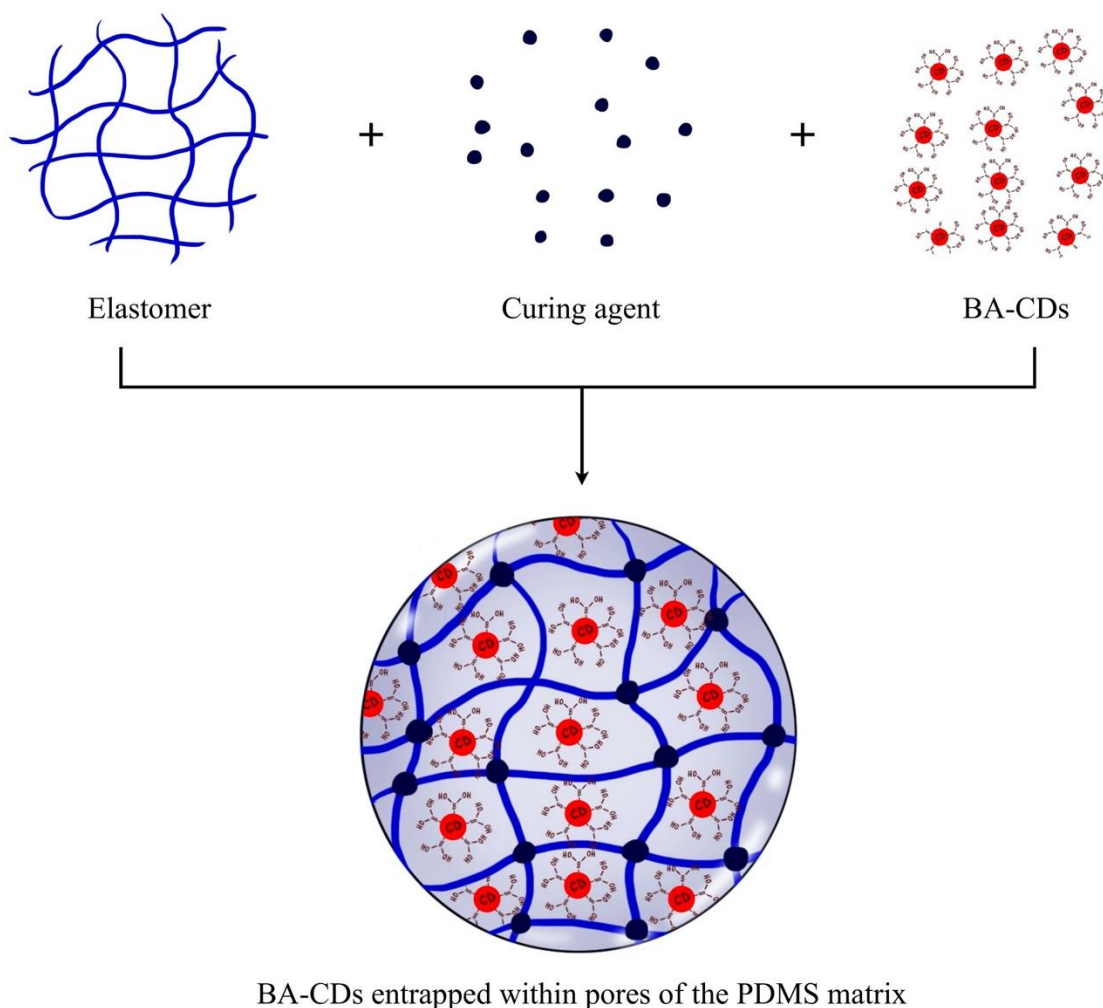


Figure 1.1 BA-CDs entrapped within pores of the crosslinked polymer chains (PDMS)

The objectives of this thesis are to: (i) fabricate and characterize BA-CD-incorporated PDMS electrodes, (ii) evaluate their electrical properties in terms of bulk impedance, conductivity, impedance at 1 kHz, and charge storage capacity, (iii) measure quantitatively their elasticity (Young's modulus), (iv) study their long-term stability in terms of electrical and mechanical features, and (v) evaluate the biocompatibility of the electrodes *in vitro*. This information will be used to provide the foundation needed for future studies to transition this flexible electrode composition for implantation purposes (electrical stimulation or signal recording purposes).

1.2 Thesis Objectives

The **general objective** of this thesis is to explore the potential of utilizing BA-CDs to add conductivity to PDMS for the development of flexible electrodes. The **specific objectives** are to 1) fabricate electrodes composed of PDMS, BA-CD, and glycerol (dispersant) 2) analyze the electrical properties of the electrodes in terms of bulk impedance, conductivity, impedance at 1 kHz, and charge storage capacity, 3) analyze the elasticity of the electrodes by measuring the Young's modulus under tensile testing, 4) study the effect of varying parameters such as the ratios of each of the components, the electrode curing temperature, and the degree of PDMS crosslinking, on the electrical properties and mechanical features of the electrodes, 5) evaluate the long-term performance of the electrodes in a body-like medium in terms of electrical and mechanical features, and 6) assess the biocompatibility of the electrodes *in vitro*.

1.3 Hypothesis

In this thesis, the aim is to develop flexible, conductive, and biocompatible electrodes using the polymer PDMS and the filler BA-CDs. We are hypothesizing that by varying different parameters including the electrode composition, curing temperature, incorporation of a dispersant, and PDMS crosslinking density we will establish electrodes that are elastic, due to the presence of PDMS, and electrically conductive and capable of storing charge, due to the presence of BA-CDs. We also expect to obtain biocompatible electrodes due to the usage of biocompatible constituents.

1.3.1 Research Objective and planned work

To test the beforementioned hypothesis, BA-CDs were synthesized using the bottom-up hydrothermal carbonization method and characterized using ultraviolet visible spectroscopy, fluorescence spectroscopy, infrared spectroscopy, and scanning electron microscopy. Following that, BA-CD-doped PDMS electrodes were prepared by mixing BA-CDs and PDMS in various ratios with or without the dispersant glycerol and molded to fabricate the electrodes. The electrodes were then tested for their impedance and conductivity using electrochemical impedance spectroscopy and for their electrochemical stability and charge storage capacity using cyclic voltammetry. Furthermore, the electrodes underwent mechanical tensile testing to quantitatively

assess their elasticity by finding the Young's modulus. Post-optimization of the electrode composition to obtain the best electrical and mechanical features, the best performing electrode composition underwent long-term stability testing in phosphate buffer saline in which the electrodes' electrical properties were measured after every incubation week. The elasticity of the electrodes was evaluated post incubation to ensure maintained elasticity of the electrodes. Finally, biocompatibility testing was carried out using the MTT assay to assess the safety of the fabricated electrodes *in vitro*.

1.4 Report Organization

The rest of this thesis contains four chapters that are organized as follows:

Chapter 2 provides a literature review on the materials explored for flexible electrode-mediated tissue stimulation and/or signal recording. The discussion focuses on the suitability of PDMS as a flexible electrode base and the conductive fillers used with PDMS. It also examines the limitations associated with the previously studied conductive PDMS-based electrodes. This chapter then analyses the potential of utilizing BA-CDs as conductive, biocompatible fillers for PDMS-based electrodes and concludes by stating the novelty of the presented work.

Chapter 3 discusses the experimental methodology used to complete the objectives of this thesis.

Chapter 4 presents and critically analyses the results obtained in this thesis.

Chapter 5 concludes this work and discusses possible future work.

Chapter 2. Literature review

This chapter explores the different flexible implantable electrodes studied for tissue stimulation and neural signal recording purposes. The chapter discusses peripheral nerve injuries as one possible application to this work. The criteria needed to qualify an electrode for body implantation are then reviewed. The progress with non-PDMS-based flexible implantable electrodes is then discussed, followed by flexible PDMS-based electrodes for tissue stimulation and/or signal recording. The chapter concludes by introducing boronic acid-modified carbon dots as suitable potential PDMS fillers to develop highly flexible, conductive, and biocompatible electrodes for future body implantation purposes.

2.1 Peripheral Nerve Injuries

The nervous system is an electrically driven system with the ability to rapidly perceive and respond to external and internal stimuli, thereby maintaining the body's homeostasis and controlling its voluntary and involuntary activities [3]. Anatomically, the NS consists of the central nervous system (CNS), composed of the brain and spinal cord, and the peripheral nervous system (PNS), composed of nerves arising from the brain and the spinal cord [26]. The PNS connects the CNS to the rest of the body by carrying information to and from the CNS via a vast network of peripheral nerves, thereby keeping the CNS constantly linked to the rest of the body [26], [27], [4]. Peripheral nerves are characterized by their fragile and delicate nature, thereby making their injury, called peripheral nerve injuries (PNIs), common under harsh conditions such as compression and bone fracture [4], [28]. Post-injury, the peripheral nerves possess the ability to regenerate, however, this process is rather slow, extending by only 1-3 mm per day [4]. Due to this slow regeneration, the target organ of the nerve (e.g. muscle) undergoes extended periods free of electrical stimulation. In the case of muscles, this leads to irreversible death or "atrophy" of the muscle [4]. To prevent muscle atrophy due to PNIs, a strategy to stimulate the muscle during the peripheral nerve regeneration is needed. This strategy also has to be capable of recording the activity of the muscle during stimulation to ensure proper contraction of the muscle [29], [30]. A promising potential strategy to treat muscle atrophy resulting from PNIs is provided by implantable electrodes as discussed in the next section.

2.2 Flexible Implantable Electrodes

Electrodes are electrically conductive materials through which electrons flow, thereby establishing an electric current [25]. When implanted within the body, those electrodes could serve as *bioelectrodes* to electrically stimulate tissues or as *biosensors* to measure and record electrical activity of tissues [31]. Such implantable electrodes are currently being increasingly investigated as potential solutions to treat conditions involving nerve damage such as PNI-induced muscle atrophy [29], [30]. Although proper functioning of the electrodes depends mainly on the choice of the electrode material [31], implantation within the body introduces several additional strict criteria that need to be considered to possibly allow future use of implantable electrodes in the clinic. Important implantable electrode features that need to be considered and satisfied include:

- 1) Low penetrability to water: penetration of water into the electrode from the wet physiological environment can disturb the adhesion between the electrode constituents and adversely influence the electrode's impedance and functioning [32].
- 2) Relatively high flexibility: lack of elasticity of the electrode implant could result in tissue and electrode damage due to the electrode-tissue mechanical mismatch. Furthermore, movement of the electrode implant could induce an inflammatory response that could impede the electrode's activity. Thus, interest has been shifting toward the utilization of materials with a relatively low Young's modulus (high flexibility) to develop implantable electrodes [5].
- 3) Biocompatibility: unlike surface electrodes, the location of implantable electrodes within the body necessitates their biocompatibility to avoid harming the body tissues [5].
- 4) Conductivity with low impedance: this would allow the smoother transmission of electric current [5].

Although the conventionally used noble metal and metallic alloys satisfy most of the conditions of implantable electrodes, they fail when it comes to mechanical match with the body tissues [5], [7]. As alternatives to metal-based electrodes, conductive, flexible implantable electrodes (FIEs) that could achieve a suitable match between the biological tissue and the electrode were studied by several groups. For instance,

flexible microelectrode arrays composed of the biocompatible polyimide onto which gold wiring has been printed were studied for the stimulation and activity recording of muscles suffering from PNI. In mouse models, the polyimide-based microelectrode with a Young's modulus of 1.67 GPa, prevented PNI-induced muscle atrophy while also effectively recording muscle activity (electromyography) [29]. Another flexible polymeric microelectrode composed polyimide, parylene and poly(3,4-ethylenedioxythiophene):poly(sodium 4-styrenesulfonate) (PEDOT:PSS) were studied for electromyography of stimulated muscles. Compared to gold electrodes, the electrochemically stable polyimide/parylene/PEDOT:PSS microelectrodes, which had an elasticity modulus of 4.62 GPa, had reduced impedances at a range of frequencies including 1 kHz and a higher CSC. In mouse models, the electrodes efficiently measured muscle activity and enhanced the signal-to-noise ratio of the recorded electromyography [30]. Flexible microelectrodes were also studied for neural recording purposes. For instance, flexible silver nanoparticle-printed polyimide nanofibers coated with PEDOT:PSS were reported to achieve stable, durable electroneurography *in vivo* [33]. Conductive carbon nanotubes (CNTs) have been combined with PEDOT-polyethylene glycol (PEDOT-PEG) and silicone insulated with fluorosilicone and reported to have impedances comparable to that of the conventional stainless steel electrodes. *In vivo*, the CNT-incorporated electrodes efficiently stimulated muscles at a lower threshold, and maintained their electrical performance over a 4 weeks interval. Furthermore, the electrodes had a low Young's modulus of 804 ± 99 kPa which resulted in a reduced inflammatory response and electrode fibrous encapsulation compared to stainless steel electrodes [34]. A summary of some implantable electrodes used for tissue stimulation and/or signal recording is provided by Table 2.1. Based on the available literature, PEDOT:PSS and polyimide seem to currently be the most commonly studied polymers for the development of flexible implantable electrodes. However, both PEDOT:PSS and polyimide are still stiffer than tissues with Young's moduli ranging between 0.8 and 2.4 GPa [35] and 2.8 GPa [36], respectively. Furthermore, although those studies utilize inherently biocompatible constituents, many do not evaluate the biocompatibility of the final composite *in vivo*. Additionally, in terms of progress to the clinic, based on the [ClinicalTrials.gov](https://www.clinicaltrials.gov) registry of clinical trials, no trials for flexible implantable electrodes are currently available although many are available for other implantable electrodes. This

search through the [ClinicalTrials.gov](https://clinicaltrials.gov) database was conducted using the following keywords “[flexible implantable electrodes](#)”, “[flexible electrodes](#)”, and “[implantable electrodes](#)”. No medical condition was specified in the search. Therefore, despite being quite promising, a lot of work is yet to be done for FEIs to be applicable for clinical use. This includes finding more flexible alternatives for a better tissue-electrode match and incorporating long-term *in vivo* biocompatibility assessment in the available literature.

2.3 PDMS-Based Elastomeric Electronics as Implantable Electrodes

Polydimethylsiloxane (PDMS), a silicone characterized by its relatively low Young’s modulus (high flexibility) that is comparable to that of biological tissues, has been utilized for the fabrication of elastomeric electronics for implantation purposes [37], [32]. Compared to other polymers, PDMS has a notably higher elasticity making it more advantageous for tissue implantation [37], [6]. Furthermore, PDMS is highly biocompatible, inert in biological environments, cheap, durable over years of implantation [9]–[11], and water impermeable, a feature especially useful in the body’s wet environment [9]–[11], [38]. However, despite its advantages, PDMS lacks the electrical conductivity required of a typical electrode to perform its sensing/stimulatory functions [16]. To compensate for its low conductivity, PDMS has been combined with several electrically conductive materials to endow the polymer with electrical conductivity [32], [37], [39]. Several studies reported the fabrication of electrically conductive PDMS by adding conductive fillers such as metals and metal oxides including silver nanowires, titanium oxide [12], [19], [40] conductive polymers such as PEDOT and polyaniline [41], [21], and carbon-based nanomaterials such as CNTs [39]. Incorporating those fillers enhanced conductivity, reduced impedance, and increased charge storage capacity while retaining the PDMS-characteristic elasticity. For instance, CNT-incorporated PDMS composites were reported to have a performance comparable to that of the conventional platinum electrodes however with a high flexibility. The CNT/PDMS electrodes effectively stimulated neuronal activity *in vivo*. This study also evaluated *in vitro* cytotoxicity and reported biocompatibility of the composite material [39]. Table 2.1 summarizes some of the studied PDMS- and non-PDMS-based implantable electrodes used for tissue stimulation and/or signal recording

purposes. Although providing promising results, the studies investigating PDMS-based electrodes suffer limitations associated with the conductive materials added. For instance, the use of PANI with silicone can reduce the elasticity of the final composite due to the semi-flexible nature of PANI [23]. The same applies to conductive polymers such as PEDOT:PSS which have elastic moduli between 0.8 and 2.4 GPa [35]. Furthermore, like with other FEI's, there is a gap in the literature in terms of safety of the conductive PDMS-based implantable electrode composites *in vivo*.

One type of non-metallic, biocompatible, and conductive material that can be explored as a PDMS filler to provide it with electrical conductivity while preserving its flexibility are carbon dots, which are described in the next section.

Table 2.1 Some implantable electrodes used for tissue stimulation and/or signal recording in the literature

Polymer	Non-polymeric additives	Young's modulus	Application	<i>In vitro/in vivo</i> biocompatibility	Ref.
Polyimide	Gold wiring	1.67 GPa	Muscle tissue stimulation and electromyography	—	[29]
polyimide, parylene, PEDOT:PSS	—	4.62 GPa	Electromyography of stimulated muscles	Biocompatible <i>in vitro</i>	[30]
polyimide nanofibers coated with PEDOT:PSS	Silver nanoparticles	41±4.1 MPa (polyimide nanofibers alone)	Electroneurography	Biocompatible <i>in vivo</i>	[33]
PEDOT-PEG, silicone, fluorosilicone insulation	CNTs	804 ± 99 kPa	Muscle stimulation	Reduced inflammation and improved tissue healing <i>in vivo</i>	[34]
Polyolefin coated with PEDOT:PSS	—	—	Peripheral nerve regeneration and stimulation	—	[42]

PEDOT:PSS, polyimide	Platinum	—	Activation of the auditory system and recording the evoked responses	—	[43]
PDMS	CNTs	3.6 ± 0.5 MPa	Neuronal stimulation and signal recording	Biocompatible <i>in vitro</i>	[39]
Commercial silicone*	TiO ₂	32.9 ± 5.01 kPa	—	—	[19]
PDMS	Silver nanowires	—	Electrical stimulation of cell proliferation and axon outgrowth	Biocompatible <i>in vitro</i>	[40]
Commercial silicone, polyaniline*	—	0.1468 MPa	Electrocardiography	—	[21]

* *Designed for future implantation purposes*

2.4 Electrically Conductive Boronic Acid-Modified Carbon Dots as Potential PDMS Fillers

Due to their attractive combination of properties, carbon-based nanomaterials have become increasingly investigated for biomedical applications. Carbon-based nanomaterials such as graphene, carbon nanotubes, and carbon dots are characterized by their high electrical conductivity, chemical stability, luminescent properties, and biocompatibility [44]. Carbon dots (CDs) are a type of sp^2 hybridized, quasi-spherical 0D carbon-based nanomaterials possessing sizes generally below 20 nm. CDs are characterized by their fluorescent properties, biocompatibility, cheap sources [45], and easy surface functionalization [46]. Since their accidental discovery in 2004, CDs have found applications in numerous areas of medicine such as imaging [47], [48], drug delivery [49], and even as electrode fillers for biosensing applications [50], [51].

Although conductive on their own, CDs' conductivity can be further enhanced by modifying the CDs with functional groups that can boost their conductivity. One such modification that could possibly enhance their conductivity involves functionalizing the CDs surface with boronic acid. Boronic acid-modified carbon dots (BA-CDs) are expected to possess superior conductivity due to the presence of Boron. Boron is one of the elements that do not obey the octet rule in that its complete valence shell consists of 6 electrons rather than 8. Therefore, Boron holds empty orbitals lacking electrons [52]. Such empty electron sites, called *holes*, are capable of carrying electrons if supplied by them. Holes like electrons are considered charge carriers through which an electric charge can pass [53]. Therefore, when supplied with voltage, the moving electrons have a vacant location to jump into. As electrons move, holes shift locations with them thereby allowing the continuous movement of charge carriers (Figure 2.1). Since electricity conduction is basically the movement of charge carriers [53], boronic acid will function to increase the electrical conductivity of the CDs. As previously discussed, a higher conductivity is desirable for better performance of the implantable electrodes. Furthermore, BA-CDs biocompatibility has been reported in the literature thereby adding to their advantages as suitable potential electrode fillers [54]. So far, several studies explored the use of BA-CDs for sensing application such as detection of glucose [55], [56] and disease-associated sialic acid [57]. However, to our knowledge, BA-CDs as electrode filler materials for tissue

stimulation and/or signal recording using surface or implantable electrodes have not been explored in the literature up until now.

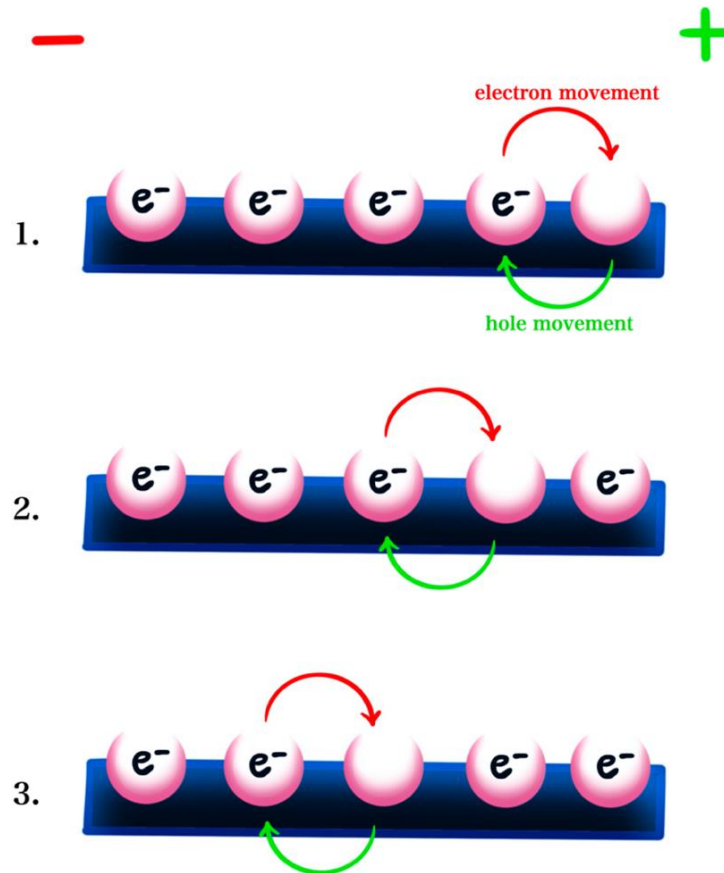


Figure 2.1 Electron-hole movement. As voltage is applied, the hole shifts towards the negative terminal while the electron moves toward the positive terminal. As the electrons move to accommodate the hole, the location of the holes shifts in the opposite direction. The movement of electrons/holes contributes to the current flow.

Several works utilized intrinsically conductive polymers (such as PANI) or non-conductive polymers combined with conductive fillers, mostly metal-based fillers such as TiO_2 , to achieve electrically conductive implantable electrodes. Using a biocompatible polymer (PDMS) with a much lower modulus of elasticity and avoiding the use of any rigid fillers by using the non-metallic BA-CDs as the conductive fillers could overcome limitations associated with the previously described studies. To our knowledge, BA-CDs have not been reported before to be used for implantable electrode applications. Therefore, the work presented in this thesis investigates for the first time

the feasibility of fabricating BA-CD-incorporated PDMS electrodes for future stimulatory and/or sensing applications.

Chapter 3. Methodology

This chapter describes the detailed methodology which explains the procedures followed for the preparation and characterization of bare BA-CDs and BA-CD-incorporated PDMS composites, electrode stability testing, biocompatibility testing, and electrophysiological signal recording experiments. Theory and reasoning behind every experiment is also provided.

3.1 Experimental protocols

3.1.1. Boronic acid-modified carbon dots (BA-CD) synthesis.

In this work, BA-CDs were synthesized using the bottom-up hydrothermal carbonization method followed by Shen et al. [56] using phenylboronic acid (PBA) as a carbon source. First, 0.4 g PBA was dissolved in 38 mL milli-Q water and then adjusted to a pH of 9.0 with 2 mL 1 M NaOH. The solution was then degassed using nitrogen gas for 1 hour, transferred to a hydrothermal vessel, and heated to 160°C for 8 hours. After cooling at room temperature, the obtained BA-CD solution was lyophilized to get dry BA-CDs.

3.1.2. BA-CD characterization.

To confirm their synthesis, BA-CDs were characterized structurally and elementally using infrared spectroscopy, ultraviolet-visible spectroscopy, fluorescence emission spectroscopy, scanning electron microscopy, and energy dispersive X-ray analysis each of which are explained below.

3.1.2.1. Infrared (IR) spectroscopy.

Figure 3.1 shows a schematic representation of the theory behind IR spectroscopy. IR spectroscopy involves exciting molecules with photons in the IR range. Upon excitation with IR photons, the different bonds of the molecule absorb some of the photons to undergo molecular vibrational transitions. Those absorbances translate into a spectrum of peaks at particular wavelengths that serve as a fingerprint for the functional groups present in molecules [58]. In this work, infrared spectroscopy was used to confirm the presence of BA-CD's functional groups: OH, BO, and CB [56].

IR spectroscopy was conducted using the Perkin-Elmer FT-IR spectrometer with an attenuated total reflectance (ATR) accessory unit.

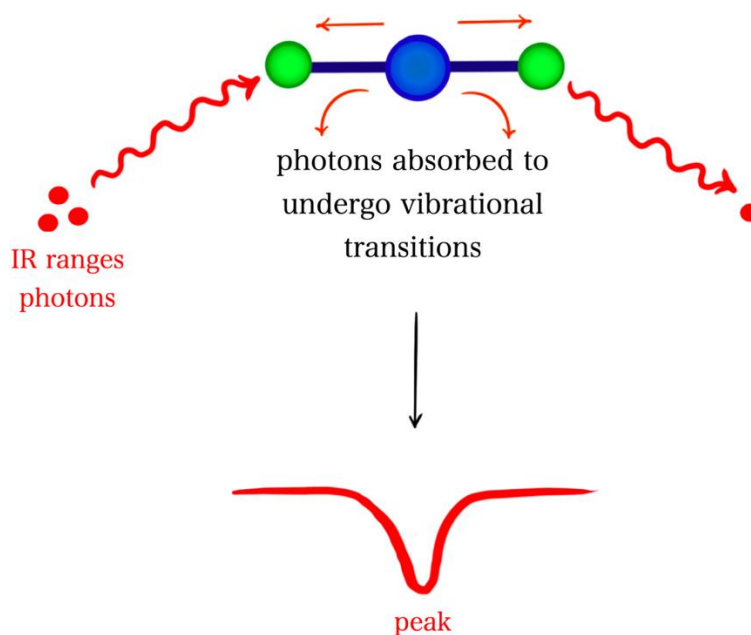


Figure 3.1 IR spectroscopy theory. When exposed to photons in the IR range, the molecule's different bonds absorb some of the photons to undergo molecular vibrational transitions. The absorbed photons translate into fingerprint peaks that represent different functional groups on the IR spectrum

3.1.2.2. Ultraviolet-visible (UV-vis) spectroscopy.

Figure 3.2 shows a schematic representation of the theory behind UV-vis spectroscopy. UV-vis spectroscopy is a type of absorption spectroscopy in which molecules are exposed to light in the UV-vis region. Upon absorption of the UV-vis light, the molecule's electrons are excited and undergo electronic transitions to higher electronic levels. This photon absorption is indicated by a hump on the UV-vis spectrum of the molecule and can serve as an indication of the identity of molecule being examined [59]. BA-CDs were reported in the literature to possess a characteristic peak at a wavelength slightly greater than 250 nm [56]. In this work, the absorption

spectrum of BA-CDs was measured to confirm BA-CD synthesis using the Shimadzu UV-1800 spectrophotometer.

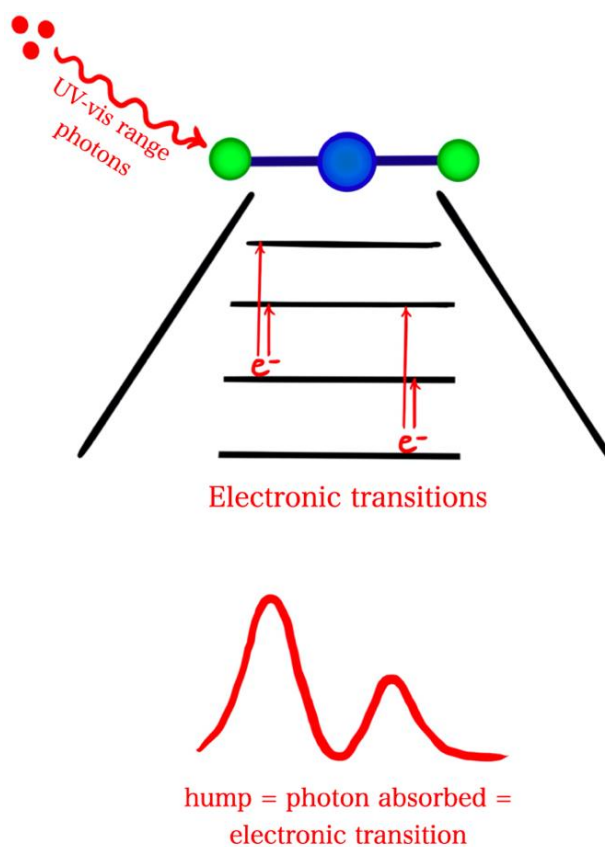


Figure 3.2 UV-vis spectroscopy theory. When exposed to photons in the UV-Vis range, the molecule's electrons absorb the photons to undergo electronic transitions. This photon absorption translates into peaks on the UV-vis spectrum that can be used for material characterization.

3.1.2.3. Fluorescence emission spectroscopy.

Figure 3.3 shows a schematic representation of the theory behind fluorescence spectroscopy. Fluorescence emission spectroscopy studies the ability of molecules to emit light upon excitation by light. More specifically, molecules are excited at the absorption/excitation wavelength, determined experimentally. After excitation, the molecules relax, emitting photons (fluorescence) which can be detected. The emission spectrum can be obtained using a fluorescence spectrophotometer [59]. Since fluorescence is one of the features of CDs, the ability of BA-CDs to fluoresce was used

to support the correct BA-CD synthesis. In this work, the emission spectrum of BA-CDs was measured using the FLSP920 series of fluorescence spectrometers.

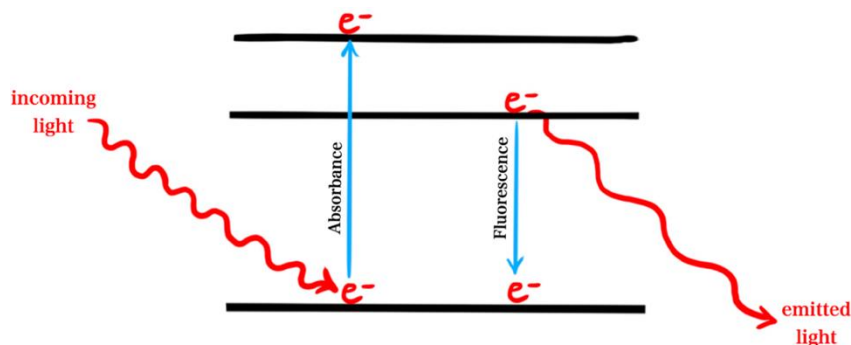


Figure 3.3 Fluorescence emission spectroscopy theory. As the molecule absorbs light, its electrons get excited after which they relax emitting fluorescence.

3.1.2.4. Scanning electron microscopy (SEM).

SEM constructs images by detecting signals emitted from samples when stroke by an electron beam [60]. The electrons emitted from different regions of the sample's surface are picked up by a detector. This allows the generation of an image with information on the topography and composition [61]. In this work, SEM was used to determine the morphology and size of the BA-CDs. BA-CDs synthesized via hydrothermal carbonization have been reported to have sizes ranging from around 2.5 nm to 6.5 nm [56].

3.1.3. Lab-scale electrode fabrication.

To fabricate the electrodes, the procedure by Alatoom et al. was followed [19] with one modification: the PDMS curing was performed *in situ* rather than using the commercial cured silicone. The composition of the electrodes was varied in terms: BA-CD percentage, Glycerol incorporation and percentage, PDMS crosslinking density (ratio of elastomer to curing agent), and electrode curing temperature. To prepare the electrodes, the silicone elastomer and curing agent were mixed in ratios of 10:1, 9:1, and 8:1. Following that, BA-CD percentages (10% and 25%) were added with or without glycerol dispersant (4%, 8%, 16%) and mixed till homogenous. The PDMS/BA-CD mixture was then molded into 3D printed circular casting trays of 1 cm

diameter and 1 mm thickness and left to cure. Figure 3.4 shows the electrode material in the casting plate (a.) and the cured electrodes (b.).

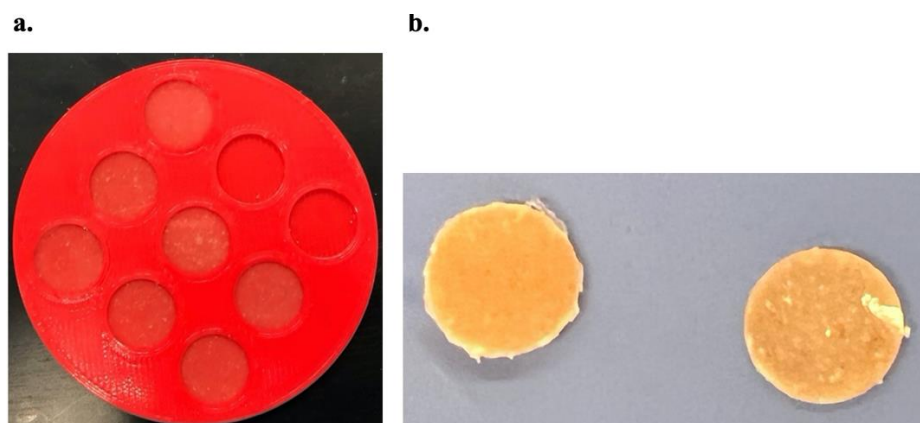


Figure 3.4 a. PDMS/BA-CD electrodes molded in 3D printed casting plates of 1 cm diameter and 1 mm thickness; b. cured electrode samples of 1 cm diameter and 1 mm thickness

The commercially available cured PDMS used in the protocol by Alatoon et al. ([19]) is a highly viscous material difficult to mix and achieve a homogenous mixture. Therefore, using uncured elastomer and curing agent both of which are liquids of much lower viscosity, makes electrode fabrication easier and is expected to achieve a more homogenous dispersion of the BA-CD filler within the PDMS.

Additionally, Figure 3.5 show the casting plates used in this work which were designed via 3D printing to overcome the limitations associated with the previously used plates. The old molds were exposed from both sides (top and bottom), making it very difficult to cast the electrodes in them. The molds used in this work have a fused base which eases the casting of the PDMS within them and avoids any leakage of the material from the plate. Furthermore, with 3D printing, plates of various shapes, sizes, and thicknesses can be easily prepared for electrode fabrication. The molds used in this study were composed of the polymer polylactic acid (PLA).

The prepared electrodes were characterized for their structure and elemental composition using ATR-IR, SEM, and EDX, electrochemical properties, mechanical flexibility, long-term stability, biocompatibility, and ability to record electrophysiological signals.

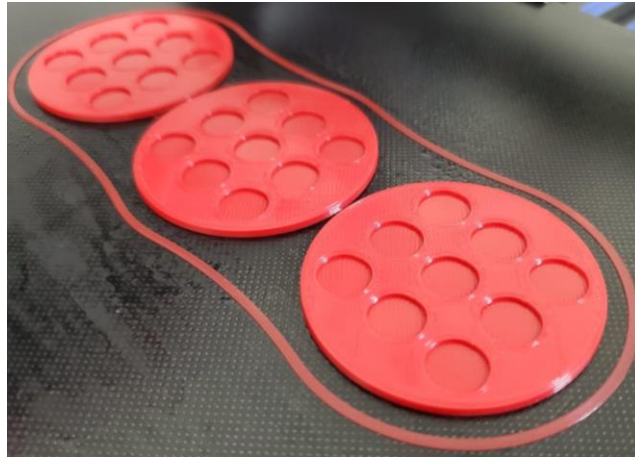


Figure 3.5 PLA casting molds with fused base; 1 cm diameter; 1 mm thickness

3.1.4. Electrochemical testing.

To study the electrochemical performance (conductivity, bulk resistance, impedance at 1 kHz, electrochemical stability, and charge storage capacity) of the fabricated electrodes, electrochemical impedance spectroscopy and cyclic voltammetry were carried out.

3.1.4.1. Electrochemical impedance spectroscopy (EIS). Electrochemical impedance spectroscopy (EIS) presents a non-destructive technique that can be utilized to measure the impedance of a system. In a typical EIS procedure, a potentiostat is used to measure impedance by applying a sinusoidal alternating potential wave of varying frequency to the working electrode and recording the resulting current wave. The frequencies can be divided into high and low regions moving from left to right on the semi-circle shown in Figure 3.6 [62].

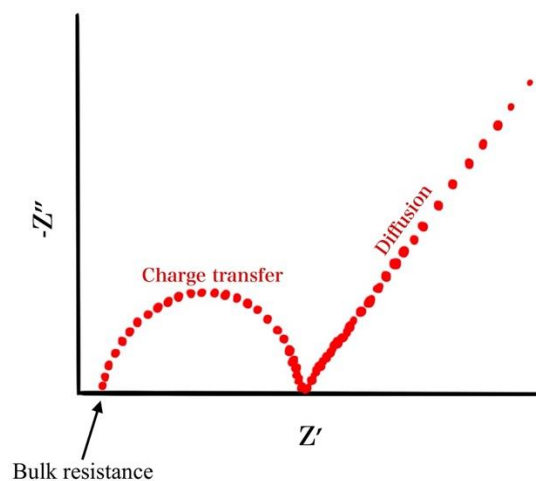


Figure 3.6 A typical Nyquist plot of a conductive material showing the charge transfer semi-circle and diffusion (Warburg impedance) line at 45°; W = Warburg; R = bulk resistance; R_{ct} = charge transfer resistance

Three values can then be calculated from the two waves:

- 1) **phase shift (Φ)** - the specific angle between 0° and 90° measured when there is a time shift between the two current and voltage waves [62].
- 2) **Real (Z') and imaginary (Z'') impedances** - real and imaginary impedances (measured in Ohms (Ω)) are obtained from the total impedance which is the ratio of the amplitude of the potential wave to the current wave. Due to the total impedance being a complex number, it has real (Z') and imaginary (Z'') components. This is also presented in the polar coordinates by Z (total impedance) being the vector length, Φ being the angle between Z and the x-axis, Z' being the x-axis and Z'' being the y-axis [62]. Figure 3.7 shows the vector representation of Z .

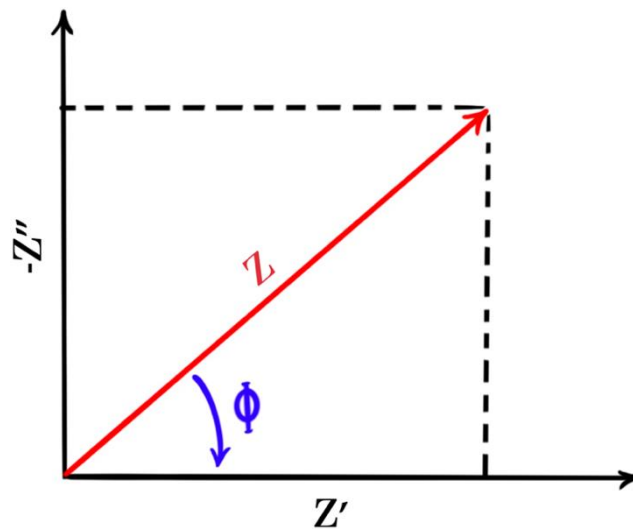


Figure 3.7 Vector representation of the impedance complex number; Z' = real impedance; Z'' = imaginary impedance

Importantly, the Z' and Z'' are used to plot the commonly used *Nyquist plot* which represents impedance as a function of Z' and Z'' . Figure 3.6 shows a typical Nyquist plot. In a Nyquist plot, Z'' represents the behaviour of capacitors while the real component Z' represents resistors that obey Ohm's law (current is proportional to voltage). The shape of the Nyquist plot is of great importance as it reflects the kinetic and transport behaviors of the system being analyzed. Different electrical circuit

compositions (capacitors and/or resistors) and arrangements (series or parallel) translate into different Nyquist plots. In the Nyquist plot presented in Figure 3.6, the first region (semi-circle) is related to *charge transfer* and its diameter corresponds to the amount of *charge transfer resistance* within the system. The second region (straight line at 45 degrees angle) represents Warburg impedance. Unlike charge transfer resistance which is related to the transfer of charges through the voids between particles, Warburg impedance results from the diffusion of the charged species. The appearance of the semicircle or the diagonal Warburg impedance line indicates which process controls charge movement in the system being tested. In addition to charge transfer resistance, EIS also can be used to obtain the value of the bulk resistance of the material tested. Bulk resistance is the point at which the semi-circle intersects the real impedance component in the high frequency region, and it indicates overall resistance of the system [62].

In this work, EIS was carried out using the *SP-200, Biologic* potentiostat shown in Figure 3.8 to measure the bulk resistance (R) and conductivity (σ) of the prepared electrodes. Furthermore, impedance of the system at 1 kHz was measured. Evaluating impedance at 1 kHz is important as it represents variations in the electrochemical responses of electrodes after periods of implantation and eases comparisons between the performances of electrodes. Electrochemical changes may take place post-implantation in scenarios such as loss of electrode of function or the formation of fibrous tissue around the electrode implant [63]. Impedance at 1 kHz is found by plotting the real impedance versus the frequency.

To conduct EIS testing, the electrodes were fabricated as disks of the same diameter as the potentiostat cell (1 cm) and 1 mm thickness. The potentiostat cell is shown in Figure 3.9. The appearance of a semi-circle in the results of the tested electrode compositions serves as a proof of conductivity while the diameter of the semi-circle (R_{ct}) indicates the amount of resistance to charge transfer. The smaller the semi-circle (smaller R_{ct} value), the lower the impedance to charge transfer. The complete absence of the semi-circle and its replacement with a vertical, stacked, or randomly scattered readings in the Nyquist plot indicates resistance and lack of conductivity. The conductivity of the tested electrodes was measured using equation 1 (eq. 1) below.

$$\sigma = \frac{t}{R \times A} \quad (\text{eq.1})$$

where,

σ = conductivity (S/cm); t = thickness (cm); R = bulk resistance (Ω); A = area (cm^2)

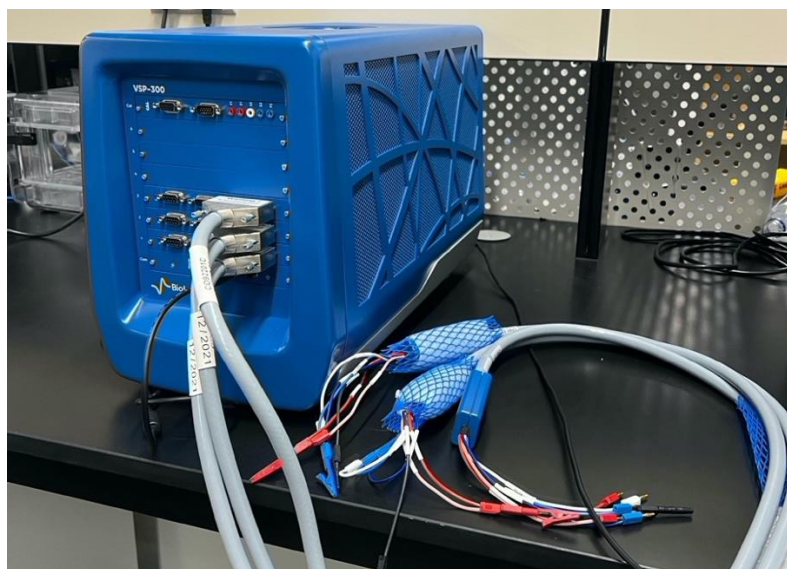


Figure 3.8 Potentiostat used for EIS studies (SP-200, Biologic)

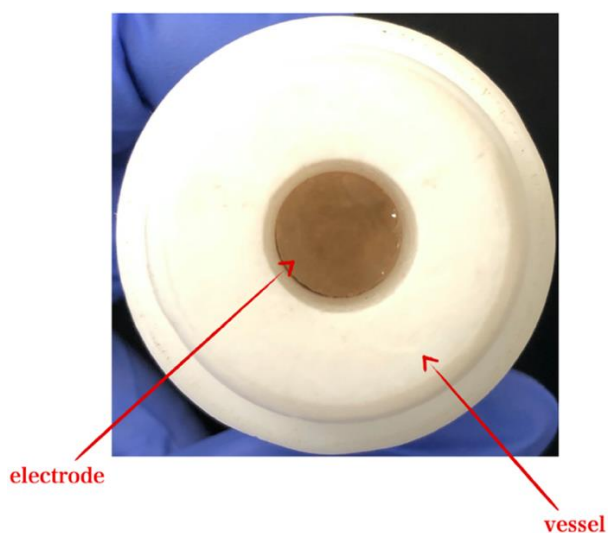


Figure 3.9 PDMS/BA-CD electrode placed in potentiostat vessel

3.1.4.2. Cyclic voltammetry (CV).

Cyclic voltammetry (CV), another widely utilized electrochemical technique, is used to qualitatively measure the stability/reactivity of a system by examining oxidation and reduction processes. In a typical CV procedure, potential is applied to the system being analyzed in one direction and then the opposite direction. The current response of the system to the reversible potential sweep is then recorded. As the potential

sweeps, the species being tested begin to oxidize or reduce depending on the direction of the potential. As the material gets oxidized or reduced, its concentration at the electrode surface changes as predicted by the *Nernst equation*. For example, when the potential sweeps negatively (high to low potential), X^+ is reduced to X . As the amount of X^+ is depleted at the electrode surface, the resulting current is measured. Once the switching potential is reached, the potential is swept in the opposite (positive) direction and X is oxidized back to X^+ . The oxidation and reduction processes that the material undergoes are presented as peaks forming a “duck-shape” on a cyclic voltammogram. Peaks on a cyclic voltammogram can be more than one on each side forming the “multiple duck shape” [64]. Figure 3.10 shows a typical duck shape and multiple duck shape cyclic voltammogram. In this work, CV was carried out using the *SP-200, Biologic* potentiostat (Figure 3.8) to study the reactivity of the fabricated electrodes. The goal of this study is to make electrochemically stable electrodes that lack any peaks in the cyclic voltammogram. Furthermore, CV was also be used to calculate charge storage capacity of the electrodes. Charge storage capacity (CSC) represents the charge built up during the reduction phase of the CV. CSC was found by computing the area below the zero baseline of voltammogram curve [30] and dividing it by the product of the CV sweep rate and the electrode area as shown by equation 2 (eq 2) below.

$$CSC = \frac{\text{area below baseline}}{\text{sweep rate} \times A} \quad (\text{eq.2})$$

where,

CSC=charge storage capacity (C/cm²); sweep rate (mV/s); A = area (cm²)

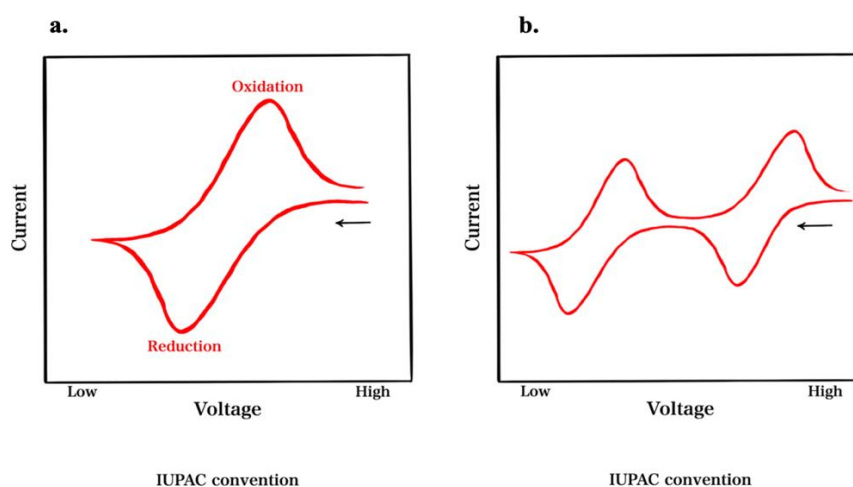


Figure 3.10 (a) typical duck shaped and (b) multiple duck shaped CV graphs

3.1.5. Mechanical testing.

To analyze the mechanical elasticity of the fabricated electrodes, mechanical tests such as tensile, compression and bending tests need to be conducted. Stress-strain curves obtained from such tests reflect various aspects of the mechanical properties of the material tested including not only elasticity but also the material's toughness, yield strength, and ultimate strength. Figure 3.11 shows a typical stress-strain curve of a material loaded till failure. In this work, the most important mechanical parameter is the elasticity of the electrodes, represented by the Young's modulus which is the slope (stress divided by strain) of the linear, elastic region of the stress-strain curve shown in Figure 3.11 [65]. In this study, tensile testing was carried out to find the Young's modulus. The obtained Young's modulus was then compared to that of some biological tissues and other flexible implantable electrodes in the literature.

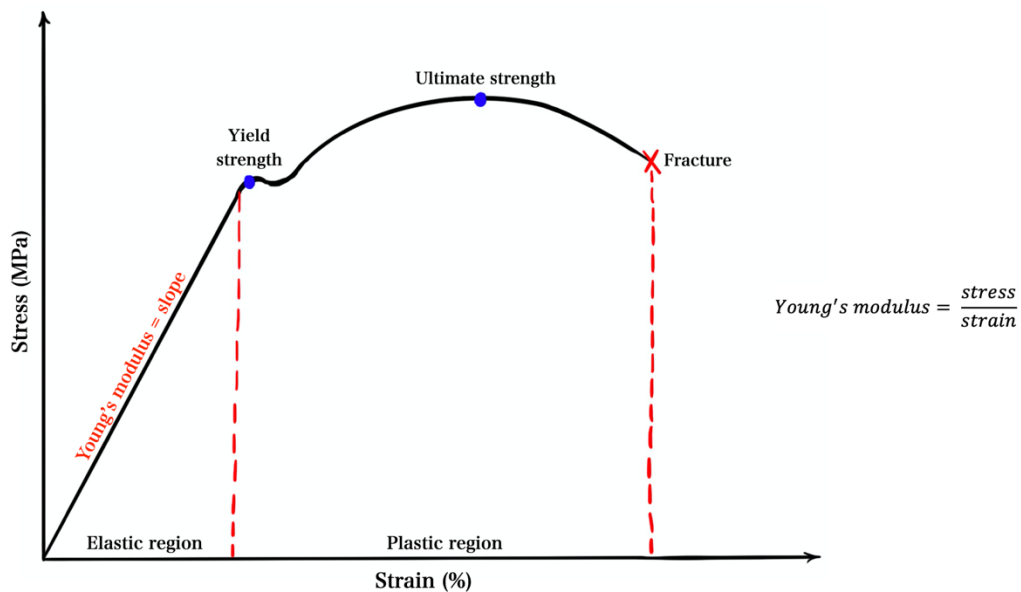


Figure 3.11 Stress-strain curve for a material loaded till failure

3.1.6. Stability testing. The stability of the electrode material was assessed by immersion in 10% phosphate buffer saline (PBS), a buffer solution with similar osmolality and ion concentration as the human body, as reported by Howlader et al. [66] and Alatoon et al [19]. The electrodes were immersed in 10% PBS solution for 12 weeks and electrochemical testing was conducted every week until the end of

the 12-week incubation period. The parameters compared before and after PBS immersion are: bulk resistance, conductivity, impedance at 1 kHz, charge storage capacity, and electrode swelling.

3.1.7. Statistical methods. For all composites prepared in this study, the conductivity, bulk resistance, and impedance at 1 kHz, and CSC were found for triplicates of each composition. The average of each of the values was found and the dispersion of the measurements from the average (standard deviation) was also obtained using excel. To ensure acceptable standard deviation, the coefficient of variance was maintained below 1. The coefficient of variance which is equivalent to the standard deviation over the mean represents the extent of spreading out of the individual values with respect to the mean. As long as the standard deviation is smaller than the mean, the coefficient of variance remains below 1 [67], [68].

3.1.8. Biocompatibility testing. To assess the biocompatibility of the electrode material, MTT assay was conducted. Figure 3.12 shows a schematic representation of the MTT assay procedure. Cells were grown until ~80% confluent and then seeded into a 96 well plate. The cells were then left again to reach ~80% cell confluency. Bare BA-CDs, glycerol, PDMS, PDMS/glycerol and BA-CD/PDMS/glycerol composites were then added to the cells seeded in the 96 well plate and incubated for the 48 hours. Upon completion of each incubation period, MTT solution was added followed by DMSO. Absorbance was then measured using the ELISA M965+ microplate spectrophotometer to calculate percentage viability. The absorbance was then used to find the percentage of the viable cells.

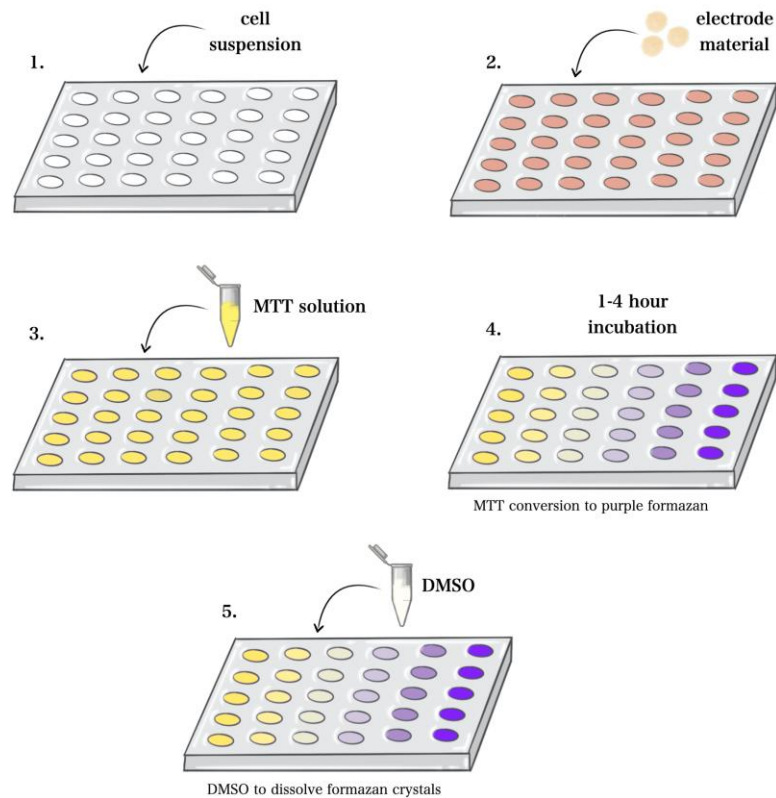


Figure 3.12 MTT assay procedure

3.1.9. Electrocardiography (ECG) and electromyography (EMG).

Electrodes used for ECG and EMG experiments were prepared using custom made molds to resemble the same structure of the commercial Ag/AgCl electrodes used for ECG and EMG readings. In those molds, the electrode mixture was cured on stainless steel as in the commercial Ag/AgCl electrodes (Figure 3.13). The cured electrodes were then used for ECG and EMG measurements and compared to the commercial Ag/AgCl electrodes.

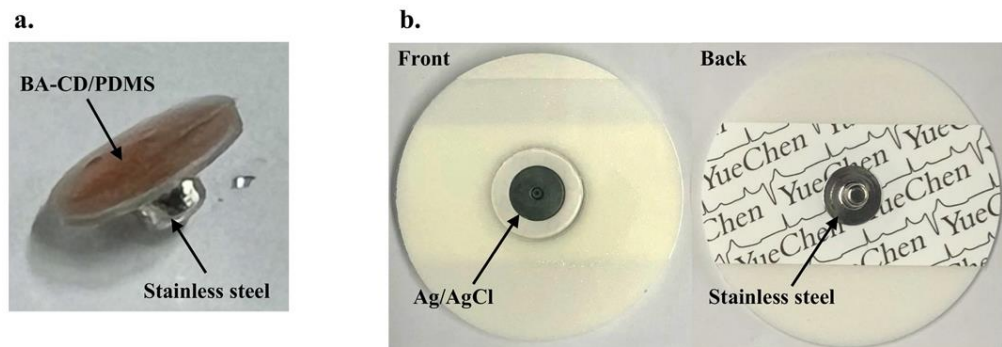


Figure 3.13 (a) BA-CD/PDMS and the (b) Ag/AgCl electrodes used for ECG and EMG measurements.

The ECG signal recorded from the two electrodes was compared using their signal-to-noise ratio (SNR) values. “PowerLab 26T” data acquisition system was used to record the lead II ECG signal using the prepared BA-CD/PDMS electrodes. The recorded ECG signal was sampled at a frequency 1 kHz/second and filtered with low pass and high pass filters at 50 Hz and 1 Hz, respectively, band stop from 49 to 51 Hz, and notch filter.

For a quantitative comparison of the signal quality, the SNR of the ECG recorded with the BA-CD electrodes and the Ag/AgCl electrodes was used. To find the SNR, the power of the signal QRS region was divided by the power of noise region between the beats. Finding the SNR was performed using MATLAB 2022b. Figure 3.14 shows a schematic explanation of the procedure used to compute the PSNR. The MATLAB code used is shown in Figure 3.15.

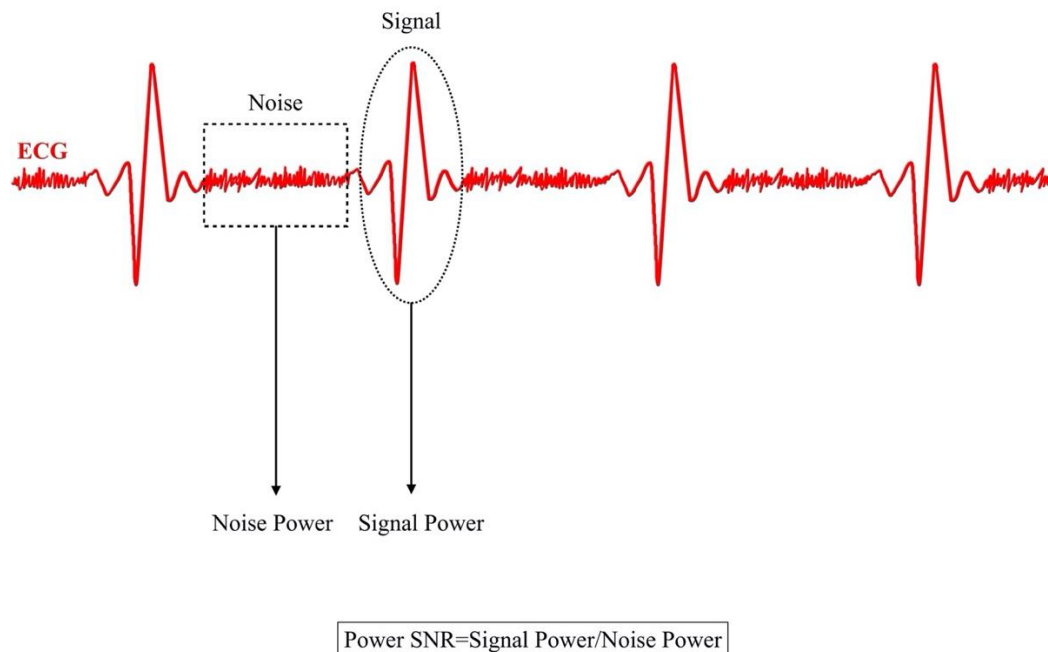


Figure 3.14 Schematic representation of the procedure used to find the SNR of the BA-CD/PDMS and the Ag/AgCl electrodes.

```

2
3 load 'AgAgCl_ECG.mat';
4 x1=1:length(data);
5 y1=data.*10^3;
6
7 load 'BACD-PDMS_ECG.mat';
8 x2=1:length(data);
9 y2=data.*10^3;
10
11 figure
12 subplot(211) %AgAgCl
13 plot(x1,y1)
14 ylabel('mV');
15 xlabel('sec');
16 title('Ag/AgCl ECG');
17 xlim([15000 20000]);
18 ylim([-1 1]);
19
20 subplot(212)
21 plot(x2,y2) %BA-CD/PDMS
22 ylabel('mV');
23 xlabel('sec');
24 title('BA-CD/PDMS ECG');
25 xlim([15000 20000]);
26 ylim([-1 1]);
27
28
29 %%Power SNR
30 %Noise
31 new_Ny1=y1(17601:17683) %Noise range of Ag/AgCl
32 new_Ny2=y2(17400:17461) %Noise range of BA-CD/PDMS electrode
33
34 Power_Ny1=sum(new_Ny1.^2); %Power of Ag/AgCl noise
35 Power_Ny2=sum(new_Ny2.^2); %Power of BA-CD/PDMS electrode noise
36
37 %Signal
38 new_Sy1=y1(17900:17982) %Signal range of Ag/AgCl
39 new_Sy2=y2(17980:18041) %Signal range of BA-CD/PDMS electrode
40
41 Power_Sy1=sum(new_Sy1.^2); %Power of Ag/AgCl signal
42 Power_Sy2=sum(new_Sy2.^2); %Power of BA-CD/PDMS electrode signal
43
44 %Power SNR = Power of Signal/Power of Noise
45 Power_SNR_AgCl=10*log(Power_Sy1/Power_Ny1)
46 Power_SNR_BACD=10*log(Power_Sy2/Power_Ny2)
47

```

Figure 3.15 MATLAB code used to find the SNR of the ECG recorded with the BA-CD electrodes and the Ag/AgCl electrodes.

To perform EMG, the differential electrodes were located on the biceps and the ground electrode on the wrist of the same arm. The EMG signal was sampled at 2 kHz/second and filtered with low pass and high pass at 2 kHz and 1 Hz, respectively, and notch. The EMG measured was then compared qualitatively to that recorded with the commercial Ag/AgCl electrodes.

Chapter 4. Results and Discussion

This chapter reports the results obtained for BA-CD characterization, characterization of the prepared BA-CD-incorporated PDMS electrodes structurally, electrochemically, and mechanically, biocompatibility analysis, and electrocardiography and electromyography recorded using the BA-CD-doped PDMS composites as surface electrodes.

4.1 Overview

BA-CDs synthesized using bottom-up hydrothermal carbonization were characterized structurally and elementally. Following that, composites composed of PDMS, glycerol, and BA-CDs of varying percentages were prepared. The degree of PDMS crosslinking was also varied in some of the compositions. The prepared composites were characterized electrochemically for their conductivity, bulk resistance, impedance at 1 kHz, and CSC, and mechanically for their Young modulus (a quantitative measure of elasticity). Biocompatibility of the prepared BA-CD/PDMS electrodes was also evaluated using MTT assay. Lastly, ECG and EMG were measured using the prepared electrodes and the signal quality was compared to that obtained using the commercial Ag/AgCl electrodes.

4.2 BA-CD Characterization

Nanomaterials can be synthesized using the bottom-up or the top-down synthesis methods. Unlike the top-down method which involves external intervention to design the nanomaterial, the bottom-up strategy involves synthesis of the nanomaterial via self-assembly of the starting molecules. The bottom-up approach is advantageous as it usually produces smaller nanoparticles at a lower cost compared to the top down-method [69]. Therefore, in this study, BA-CDs were synthesized using the bottom-up carbonization. Characterization of the prepared BA-CDs is presented in the subsections below.

4.2.1 ATR-IR spectroscopy

Figure 4.1 shows the IR spectrum of bare BA-CDs. The IR spectrum shows peaks corresponding to the presence of boron-oxygen stretching (1338 cm^{-1}), boron-oxygen-hydrogen deformation (1133 cm^{-1}), carbon-boron stretching (986 cm^{-1}), and

boron-oxygen-hydrogen deformation (942 cm^{-1}) [56], [70]. The presence of those BA-CD-characteristic functional groups provides direct evidence of the correct synthesis of carbon dots and their surface modification with boronic acid.

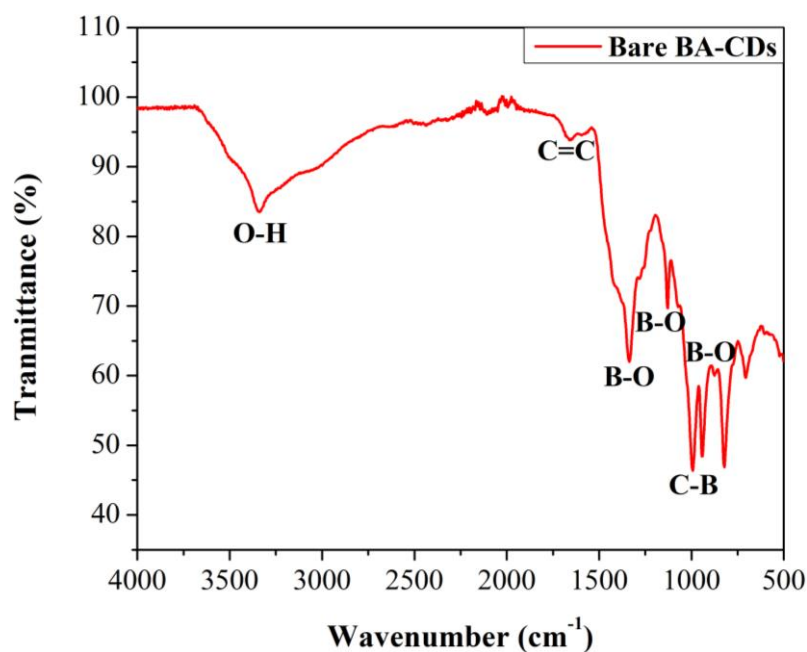


Figure 4.1 ATR-IR spectrum of bare BA-CDs

4.2.2 UV-Vis (absorption) and fluorescence (emission) spectroscopy

Figure 4.2 shows the UV-vis and fluorescence spectra of bare BA-CDs. The BA-CD UV-vis spectrum shows an absorption peak at $\sim 268.4\text{ nm}$. This peak is in agreement with that reported in the literature for BA-CDs [56]. The BA-CDs were then excited at 270 nm to evaluate their fluorescence properties. The BA-CDs emitted light (fluorescence) at $\sim 297.7\text{ nm}$. Since carbon dots are known for their ability to fluoresce, the fluorescence of the synthesized BA-CDs at $\sim 297.7\text{ nm}$ further supports the correct synthesis of carbon dots. Therefore, UV-vis and fluorescence emission spectroscopies complement the IR results in supporting the correct synthesis of BA-CDs.

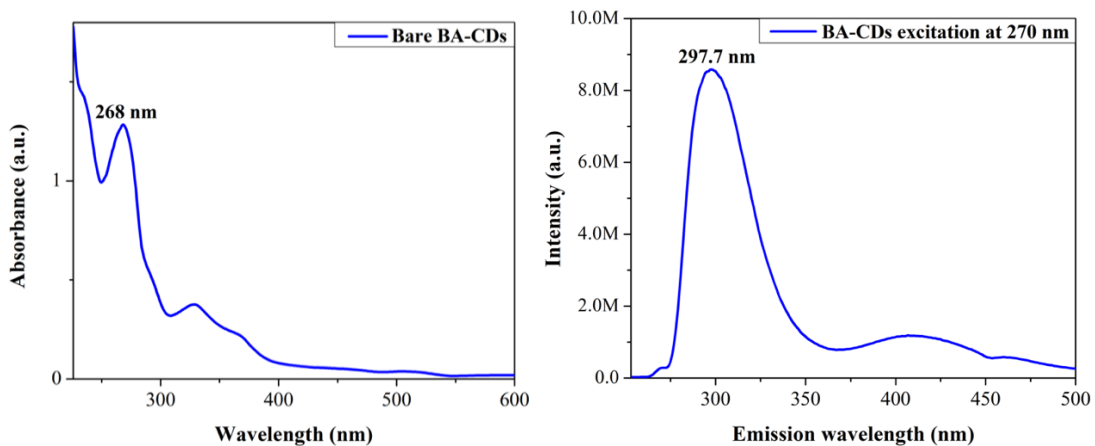


Figure 4.2 UV-vis and fluorescence spectra of bare BA-CDs

4.2.3 SEM

Figure 4.3 shows the SEM images of bare BA-CDs. The SEM images reveal the surface spherical morphology of the synthesized BA-CDs and their sizes ranging between 8 and 18 nm, approximately. Carbon dots are reported to typically have sizes smaller than 10 nm [24]. The slight increase in the diameters of the BA-CDs synthesized in this study could be due to the surface modification of the carbon dots with boronic acid. It is worth noting that SEM of BA-CDs was conducted without spraying gold onto it prior to imaging. Gold is typically used before to provide the sample with the needed conductivity for SEM imaging. This indicates BA-CDs conductivity.

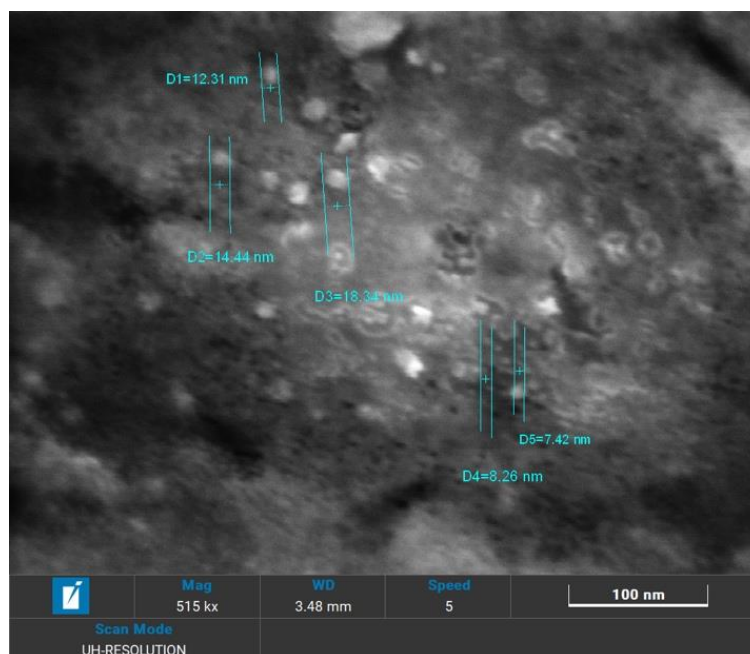


Figure 4.3 SEM image of bare BA-CDs

4.2.4 Electrochemical testing: EIS and CV

The electrochemical properties of the bare BA-CDs (conductivity, bulk resistance, impedance at 1 kHz, CSC, and electrochemical stability) were next evaluated before utilizing it as a PDMS filler. Figure 4.4 shows the Nyquist plots and cyclic voltammograms of triplicate 1 mm thick BA-CD disks. The appearance of the charge transfer semi-circle in the BA-CD Nyquist plots indicates the ability of the electrons to move between carbon dots and hence their conductivity. Quantitatively, the BA-CDs had a bulk resistance of 0.148 ± 0.137 k Ω , a conductivity of $2.28 \pm 2.02 \times 10^{-3}$ S/cm, an impedance at 1 kHz of 0.017 ± 0.014 M Ω , and a CSC of 151.1 ± 117.4 $\mu\text{C}/\text{cm}^2$.

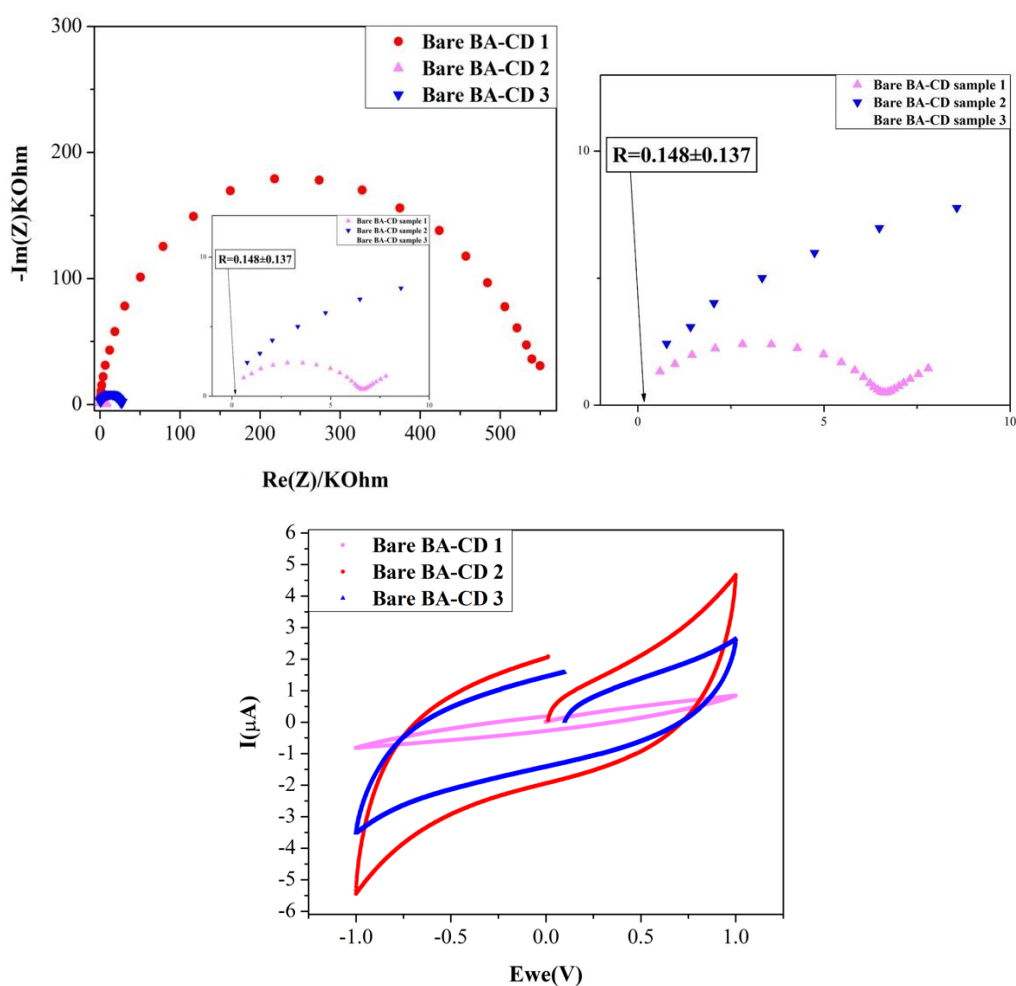


Figure 4.4 Nyquist plots (with zoomin plots) and cyclic voltammograms of triplicate BA-CD disks of 1 mm thickness

4.3 BA-CD/PDMS Composites: Characterization

The different BA-CD/PDMS composites prepared and studied are summarized in Table 4.1 below. All compositions were prepared on a mass basis. The characterization of those composites is discussed in the upcoming sections.

Table 4.1 Compositions of the electrodes prepared in this study

	BA-CDs (%)	PDMS (%)	Glycerol (%)	Crosslinking degree (elastomer to curing agent ratio)
Sample 1	10	90	0	10:1
Sample 2	25	75	0	10:1
Sample 3	10	86	4	10:1
Sample 4	10	82	8	10:1
Sample 5	10	74	16	10:1
Sample 6	25	59	16	10:1
Sample 7	10	74	16	9:1
Sample 8	10	74	16	8:1
Sample 9	25	59	16	8:1

4.3.1 ATR-IR and SEM:

Figure 4.5 shows the ATR-IR of 10% BA-CD, 4% glycerol, 86% PDMS (10:1) electrodes. The IR spectrum shows peaks corresponding to PDMS but not BA-CDs or glycerol. This could be due to the BA-CDs being imbedded within the PDMS matrix. Figure 4.6 shows the SEM images of electrodes composed of 10% BA-CD, 16% glycerol, and 74% PDMS. The SEM images show the relatively smooth surface of the electrode with very few air bubbles shown as pores in the SEM image. Compared to other flexible electrodes such as commercial silicone doped with TiO₂, BA-CD/PDMS electrodes had a smoother surface and a reduced number of air bubbles [19]. The presence of many air bubbles could impede the conductivity of the electrodes. The elemental EDX analysis shown in Figure 4.7 shows the presence of silicon (Si), carbon (C) and oxygen (O) from the PDMS. Most of the electrode is composed of Si (40.9 wt%), followed by C (33.9 wt%), and O (24.9 wt%). Boron from the BA-CDs is not detected possibly due its low weight percentage as Boron is a very small atom which

makes it difficult to detect. Furthermore, BA-CDs are embedded within the PDMS matrix also making it difficult to detect.

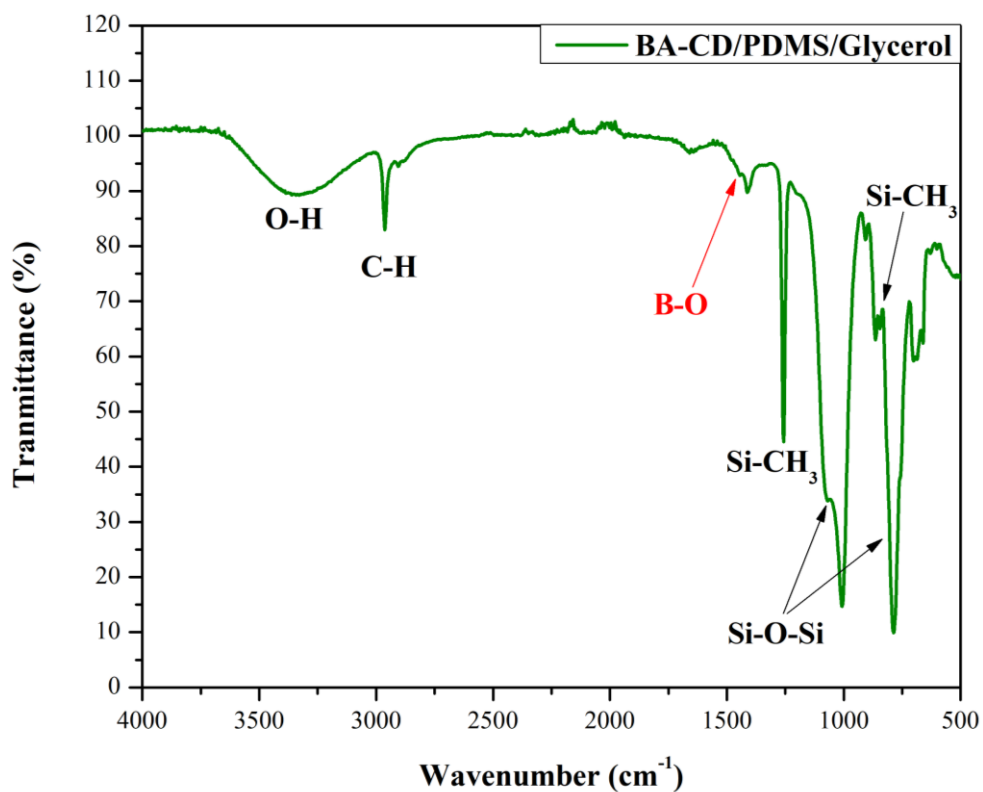


Figure 4.5 ATR-IR spectrum of 10% BA-CD, 4% glycerol, and 84% PDMS composites

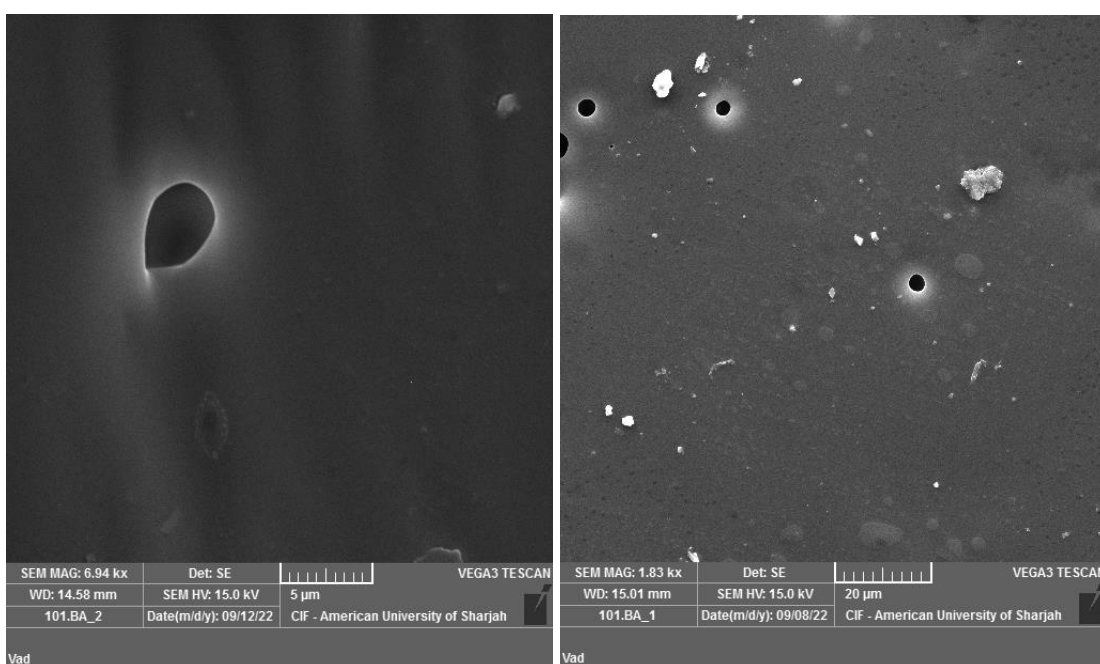


Figure 4.6 SEM image of 10% BA-CD, 16% glycerol, and 74% PDMS composites

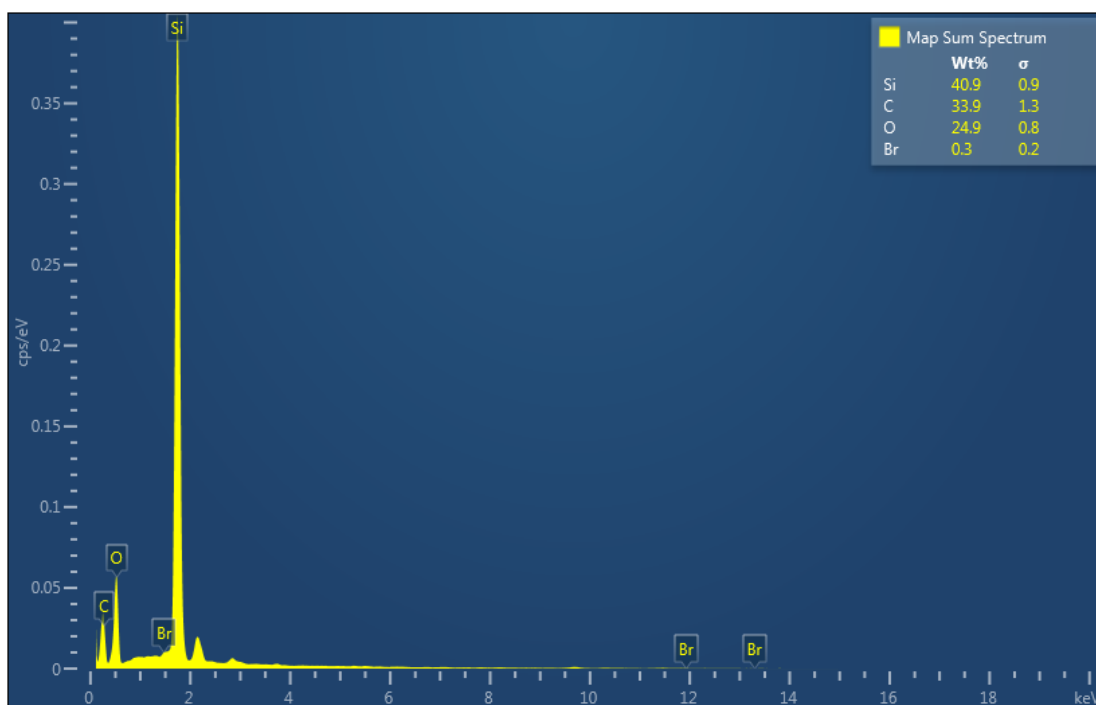


Figure 4.7 EDX elemental analysis of 10% BA-CD, 16% glycerol, 74% PDMS composites

4.3.2 Electrochemical testing: EIS and CV

The electrochemical properties of the BA-CD/PDMS composites in terms of conductivity, bulk resistance, impedance at 1 kHz, CSC, and electrochemical stability were evaluated using EIS and CV. Figure 4.8 shows the Nyquist plots and cyclic voltammograms of 10% BA-CD and 90% PDMS composites. The 10% BA-CD-doped PDMS was conductive as indicated by the Nyquist plots' semicircle and electrochemically stable as indicated by the absence of oxidation and reduction peaks in the cyclic voltammograms. Specifically, the composites had a conductivity of $5.15 \pm 2.26 \times 10^{-4}$ S/cm, bulk resistance of 0.290 ± 0.149 k Ω , impedance at 1 kHz of 3.687 ± 2.565 M Ω , and a CSC of 1.5 ± 1.1 μ C/cm².

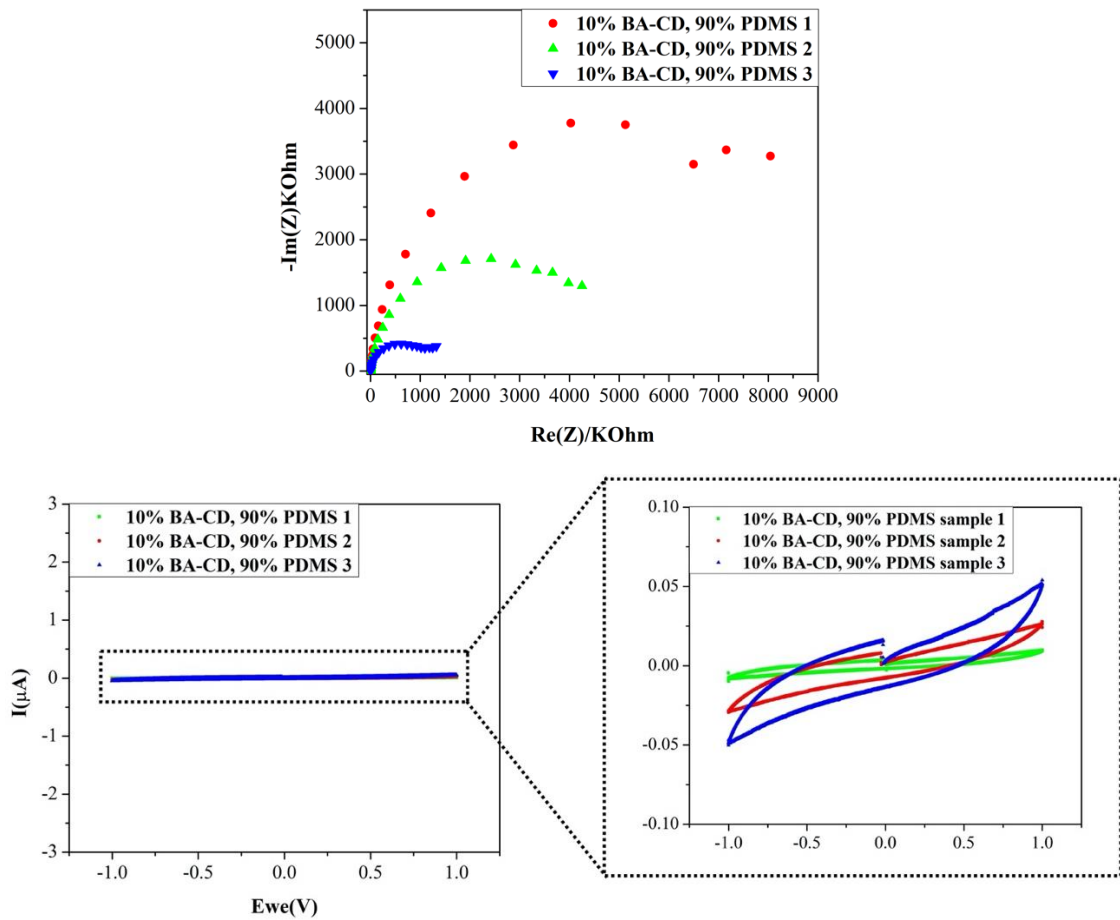


Figure 4.8 Nyquist plots and cyclic voltammograms of triplicate 10% BA-CD and 90% PDMS composites of 1 mm thickness

Figure 4.9 shows the Nyquist plots and cyclic voltammograms of 25% BA-CD and 75% PDMS composites. Increasing the BA-CD percentage to 25% negatively impacted the electrical properties as indicated by the stacking of the readings in the Nyquist plots and by the reduced current response to the applied voltage shown in the cyclic voltammograms. The deterioration of the performance could stem from the agglomeration of the BA-CDs at higher concentrations. Nanoparticles have a higher tendency to agglomerate at higher concentrations [71]. Properties and in turn performance of the nanoparticle has been reported to be affected by agglomeration, including mechanical properties [72], [71].

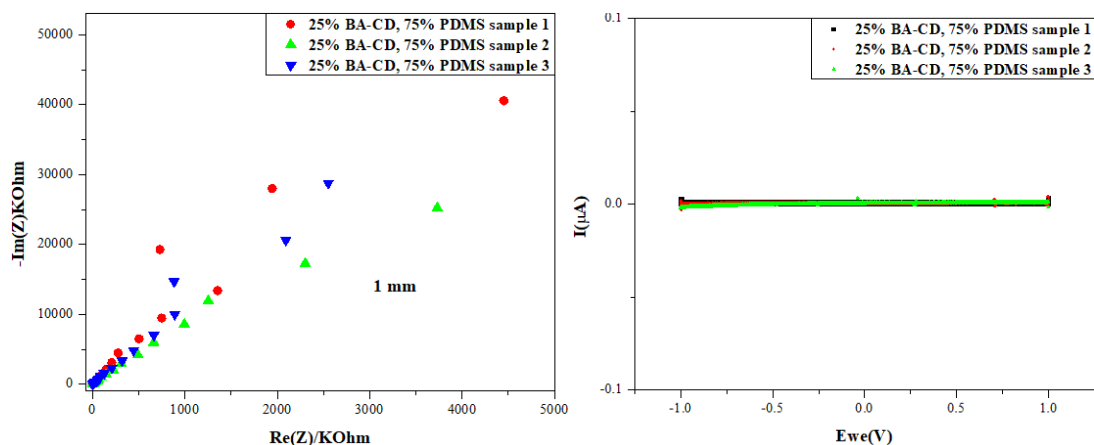


Figure 4.9 Nyquist plots and cyclic voltammograms of triplicate 25% BA-CD and 75% PDMS composites of 1 mm thickness

To assess the effect of dispersing the BA-CDs on the electrode's electrochemical performance, the dispersant glycerol was incorporated into the electrode composition at varying percentages (4%, 8%, and 16%). The electrochemical performance of the three compositions was then evaluated with EIS and CV. Figure 4.10 shows the Nyquist plots and cyclic voltammograms of triplicate 10% BA-CD, 4% glycerol, and 86% PDMS composites. The electrodes had a conductivity of $3.82 \pm 1.27 \times 10^{-4}$ S/cm, bulk resistance of 0.303 ± 0.184 k Ω , impedance at 1 kHz of 3.565 ± 1.312 M Ω , and a CSC of 1.4 ± 0.8 $\mu\text{C}/\text{cm}^2$. Figure 4.11 and 4.12 shows the Nyquist plots and cyclic voltammograms of triplicate 10% BA-CD, 8% glycerol, and 82% PDMS and triplicate 10% BA-CD, 16% glycerol, and 74% PDMS composites. Increasing the glycerol percentage to 8% improved the electrochemical parameters of the composites with a conductivity of $5.17 \pm 1.47 \times 10^{-4}$ S/cm, bulk resistance of 0.269 ± 0.085 k Ω , impedance at 1 kHz of 1.465 ± 0.477 M Ω , and a CSC of 1.7 ± 0.6 $\mu\text{C}/\text{cm}^2$. Further raising the glycerol percentage to 16% improved the conductivity ($6.75 \pm 3.30 \times 10^{-4}$ S/cm), bulk resistance (0.218 ± 0.0919 k Ω), impedance at 1 kHz (2.008 ± 1.374 M Ω), and CSC (6.8 ± 6.3 $\mu\text{C}/\text{cm}^2$). Therefore, glycerol improved the electrodes' electrochemical performance in a dose dependent manner.

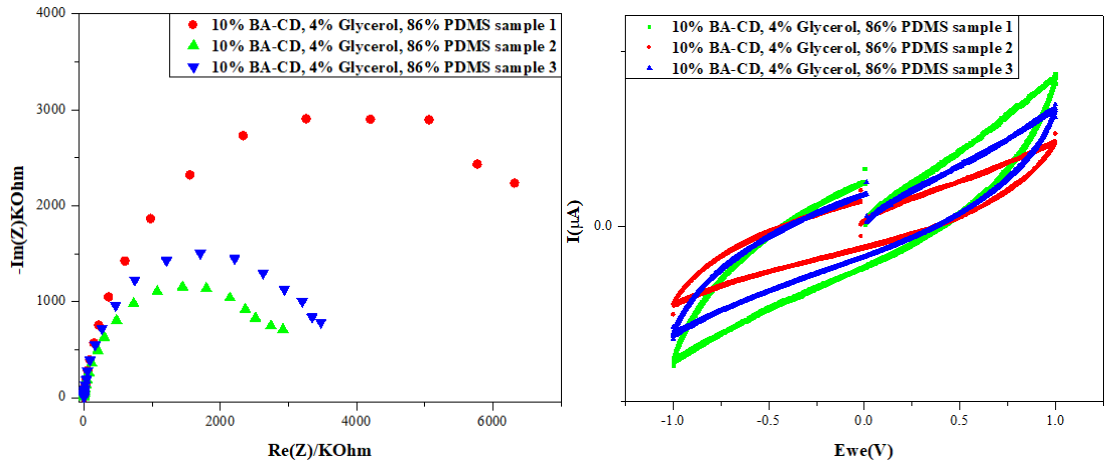


Figure 4.10 Nyquist plots and cyclic voltammograms of triplicate 10% BA-CD, 4% glycerol, and 86% PDMS composites of 1 mm thickness

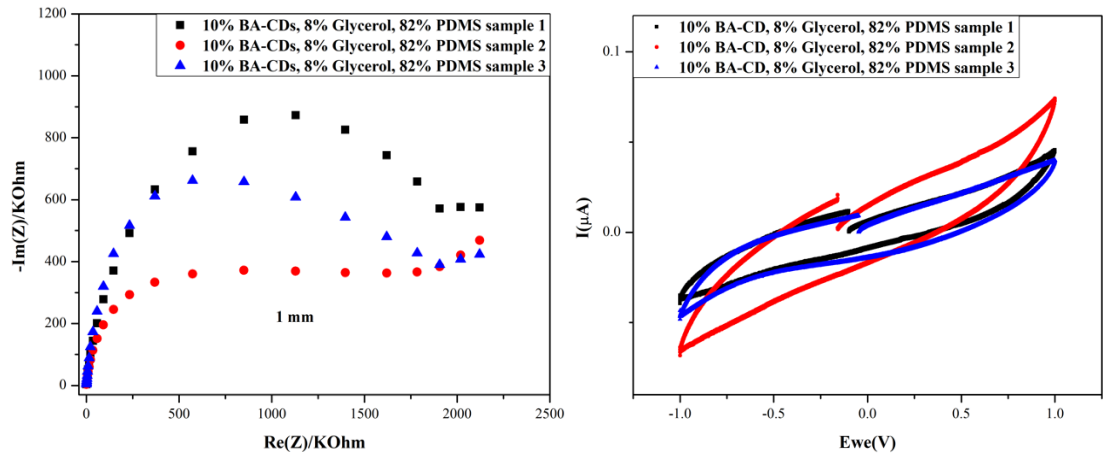


Figure 4.11 Nyquist plots and cyclic voltammograms of triplicate 10% BA-CD, 8% glycerol, and 82% PDMS composites of 1 mm thickness

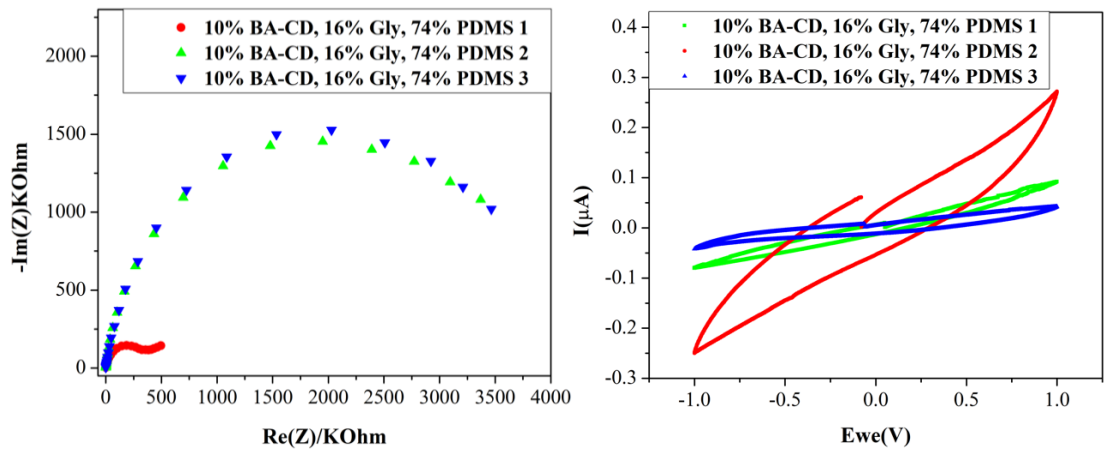


Figure 4.12 Nyquist plots and cyclic voltammograms of triplicate 10% BA-CD, 16% glycerol, and 74% PDMS composites of 1 mm thickness

Glycerol is known to possess proton conductivity [73]. Therefore, the improvements in the electrochemical features of the electrodes could stem from BA-CD dispersion by glycerol or glycerol's proton conductivity. To determine which mechanism enhanced the electrodes' performance, controls composed of glycerol and PDMS were prepared and studied using EIS and CV. Figures 4.13 and 4.14 show the Nyquist plots and cyclic voltammograms of 8 and 16% glycerol with 92 and 84% PDMS, respectively. Both compositions had poor electrical conductivity as shown by the stacking of readings in the Nyquist plots and lack of current response in the cyclic voltammograms. Therefore, the improvement in electrode performance observed with glycerol incorporation is due to BA-CD dispersion and not glycerol's proton conductivity.

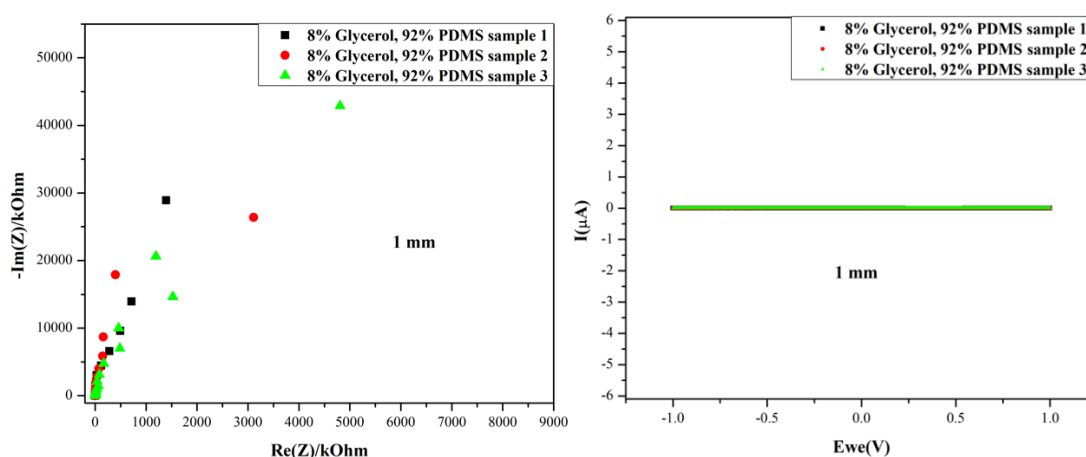


Figure 4.13 Nyquist plots and cyclic voltammograms of triplicate 8% glycerol, and 92% PDMS composites of 1 mm thickness

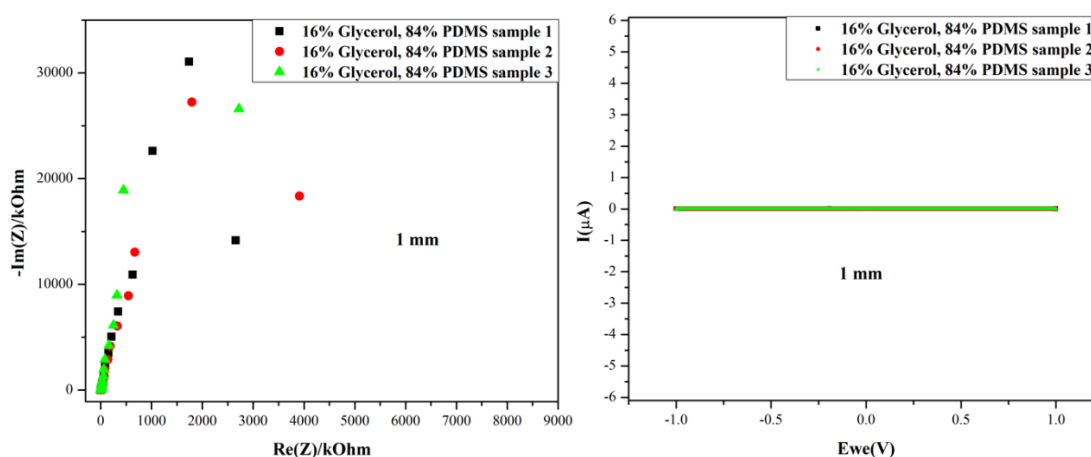


Figure 4.14 Nyquist plots and cyclic voltammograms of triplicate 16% glycerol, and 84% PDMS composites of 1 mm thickness

Next, the effect of another parameter, curing temperature, on the electrode's electrochemical properties was studied. Curing at higher temperatures has been reported to improve filler dispersion in a polymeric matrix and hence enhance the composite's electrochemical properties [74]. Furthermore, varying the curing temperature has also been reported to affect PDMS's polymeric structure [75]. This could in turn influence the composites properties such as conductivity. Therefore, the effect of a higher curing temperature on the electrochemical performance of the BA-CD/PDMS composites was studied. Figure 4.15 shows the Nyquist plots and cyclic voltammograms of 10% BA-CD, 16% glycerol, and 74% PDMS composites cured at 60°C. The composites had a poor electrical conductivity as indicated by the stacked Nyquist plot reading and the lack of current response to the applied voltage in the cyclic voltammogram. Therefore, high temperature curing negatively affected the electrochemical performance of the BA-CD/PDMS composites. Hence, from this point on, only room temperature composite curing was used.

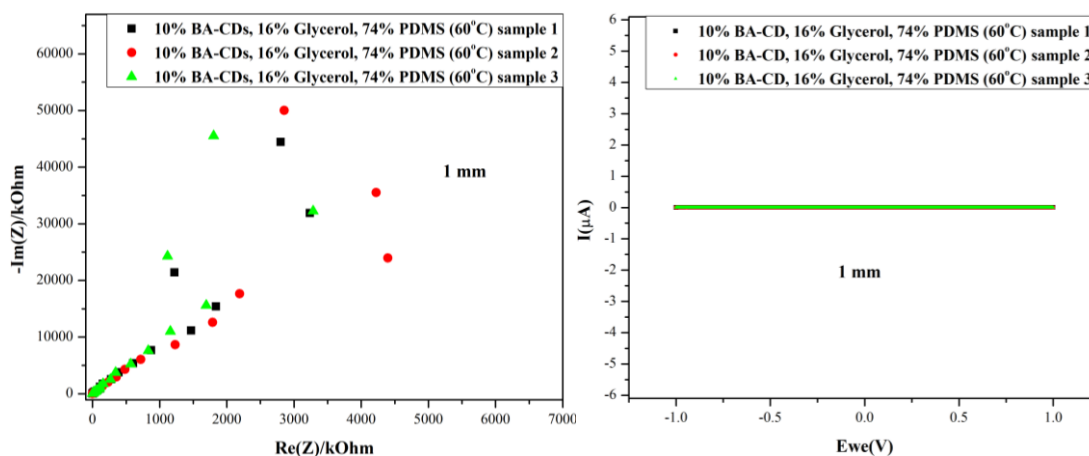


Figure 4.15 Nyquist plots and cyclic voltammograms of triplicate 10% BA-CD, 16% glycerol, and 74% PDMS composites of 1 mm thickness cured at 60°C

All composites tested so far were prepared with the usual PDMS crosslinking degree (10 elastomer to 1 curing agent ratio). This is the recommended ratio typically used in the literature [76]. The influence of increasing PDMS's crosslinking density on the composite's electrochemical performance was next assessed based on the hypothesis that higher crosslinks will bring the BA-CDs closer together thereby facilitating electron transfer and hence, increasing conductivity of the composite. Figures 4.16 and 4.17 show the Nyquist plots and cyclic voltammograms of 10% BA-CD, 16% glycerol, and 74% PDMS with 9:1 and 8:1 crosslinking ratios, respectively.

The electrochemical parameters improved with increase in crosslinking density. Specifically, the 9:1 and 8:1 crosslinked composites had conductivities of $2.48 \pm 1.88 \times 10^{-3}$ and $9.62 \pm 3.45 \times 10^{-3}$ S/cm, bulk resistances of 0.102 ± 0.0819 and 0.058 ± 0.0135 k Ω , impedances at 1 kHz of 2.37 ± 0.417 and 0.964 ± 0.361 M Ω , and CSCs of 5.8 ± 5.4 and 21.4 ± 5.9 $\mu\text{C}/\text{cm}^2$, respectively. Therefore, increasing polymer crosslinking improved the electrochemical performance of the electrodes. However, it is important to note that, increasing crosslinking density can reduce the flexibility (higher Young's modulus) of the polymer [77].

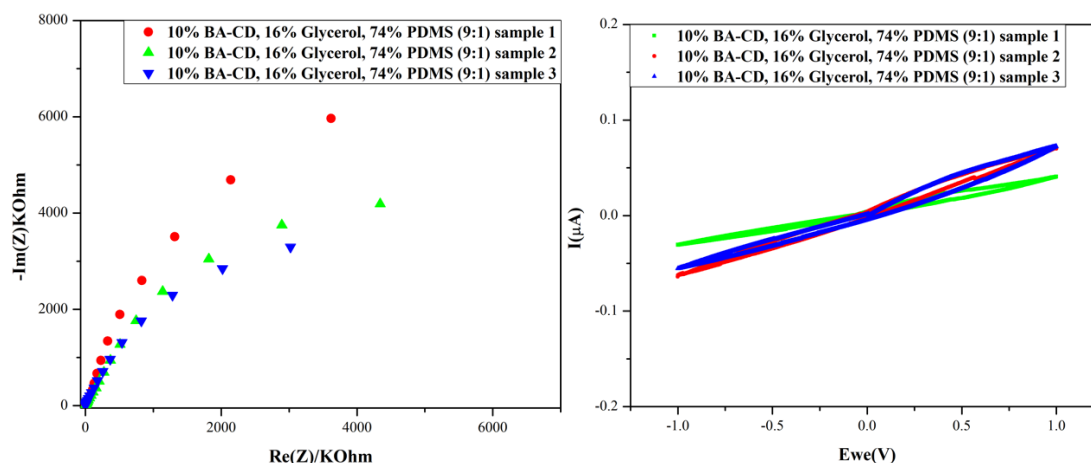
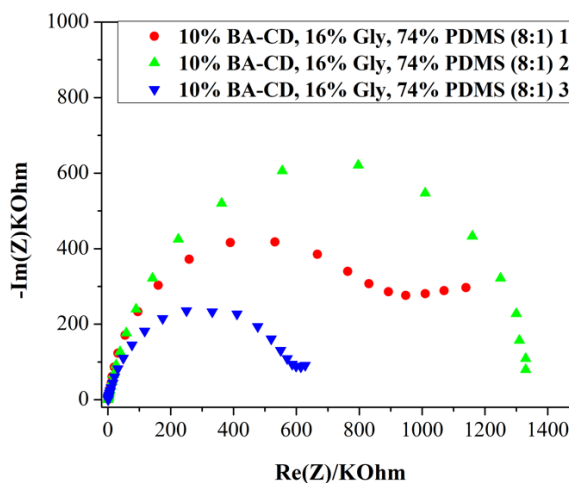


Figure 4.16 Nyquist plots and cyclic voltammograms of triplicate 10% BA-CD, 16% glycerol, and 74% PDMS (9:1) composites of 1 mm thickness



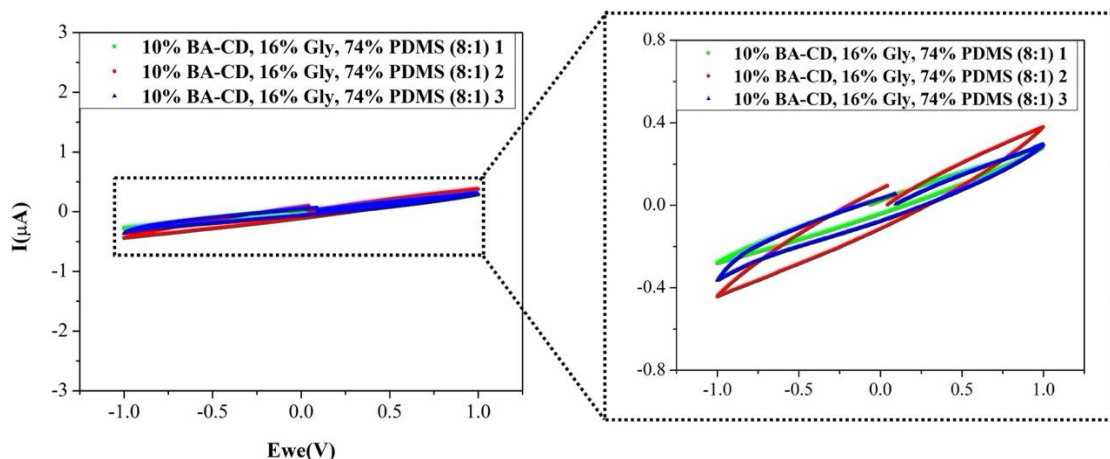


Figure 4.17 Nyquist plots and cyclic voltammograms of triplicate 10% BA-CD, 16% glycerol, and 74% PDMS (8:1) composites of 1 mm thickness

Table 4.2 summarized the electrochemical values obtained for the different BA-CD, glycerol, and PDMS compositions prepared and tested in this study.

Table 4.2 Summary of the conductivity, bulk resistance, impedance at 1 kHz, and CSC values for all the prepared and tested compositions.

#	Composite composition			Bulk resistance (kΩ)	Impedance at 1 kHz (MΩ)	Conductivity (S/cm)	CSC (μC/cm ²)
	PDMS %	BACD %	Glycerol %				
1	0	100	0	0.148±0.137	0.017±0.014	2.28± 2.02×10 ⁻³	151.1± 117.4
2	90	10	0	0.290±0.149	3.687± 2.565	5.15± 2.26×10 ⁻⁴	1.5± 1.1
3	86	10	4	0.303±0.184	3.565± 1.312	3.82± 1.27×10 ⁻⁴	1.4± 0.8
4	82	10	8	0.269±0.085	1.465± 0.477	5.17± 1.47×10 ⁻⁴	1.7± 0.6
5	74	10	16	0.218±0.092	2.008± 1.374	6.75± 3.30×10 ⁻⁴	6.8± 6.3
6	74 (9:1)	10	16	0.102±0.082	2.37± 0.417	2.48± 1.88×10 ⁻³	5.8± 5.4
7	74 (8:1)	10	16	0.058±0.014	0.964± 0.361	9.62±3 .45×10 ⁻³	21.4± 5.9

8	59	25	16	0.186±0.060	0.058± 0.016	7.51± 2.71×10 ⁻⁴	62.9± 4.6
---	----	----	----	-------------	-----------------	--------------------------------	-----------

4.3.3 Mechanical testing: tensile testing

To evaluate the flexibility of the developed electrodes and ensure it is within a range suitable for contact with body tissues, the Young's moduli of the electrodes was assessed using tensile testing. The top three performing electrodes electrochemically underwent tensile testing and their Young's moduli was found by finding the slope of the elastic region of the stress-strain curve. Table 4.3 summarizes the Young's moduli of 10% BA-CD, 16% glycerol, 74% PDMS (8:1), 10% BA-CD, 16% glycerol, 74% PDMS (9:1) and 10% BA-CD, 25% glycerol, 59% PDMS (10:1) and compares them to that of other flexible polymeric electrodes and some biological tissue. Furthermore, the Young's modulus of 10% BA-CD, 16% glycerol, 74% PDMS (10:1) was used as a control. As shown in Table 4.3, the highest flexibility was found for 10% BA-CD, 16% glycerol, 74% PDMS with 8:1 crosslinking (0.0505 ± 0.0218 MPa). This elasticity was higher than that of all polymer-based electrodes except TiO₂/glycerol/commercial silicone which had a slightly higher elasticity. Compared to biological tissues, the 10% BA-CD, 16% glycerol, 74% PDMS (8:1) electrodes were mechanically compatible with skin tissues but slightly more rigid than muscle tissues. The elastic region of the tensile stress-strain curve of triplicate 10% BA-CD, 16% glycerol, 74% PDMS (8:1) electrodes is shown in Figure 4.18. The electrodes post-rupture due to applied tensile force are shown in Figure 4.19.

Table 4.3 Some of the Young's moduli of BA-CD/PDMS electrodes, other flexible polymeric electrodes, and some biological tissues

Material	Young's modulus (MPa)	Reference
10% BA-CDs, 16% Glycerol, 74% PDMS (10:1)	0.0643±0.0498	This work
10% BA-CDs, 16% Glycerol, 74% PDMS (9:1)	0.262±0.160	This work
10% BA-CDs, 16% Glycerol, 74% PDMS (8:1)	0.0505 ± 0.0218	This work
25% BA-CDs, 16% Glycerol, 59% PDMS (10:1)	0.133±0.039	This work
TiO ₂ /Glycerol/commercial silicone	0.0329	[19]
PDMS/thin film gold	1.81±0.01	[37]

Polyimide/gold wiring	1670	[29]
PEDOT:PSS/polyimide/ parylene	4620	[30]
TiO ₂ /polymethyl methacrylate/PDMS	0.237	[78]
Skeletal muscle	0.0247 ± 0.035	[79]
Skin tissue	0.33 – 1.28*	[80]

*based on the site of skin tissue

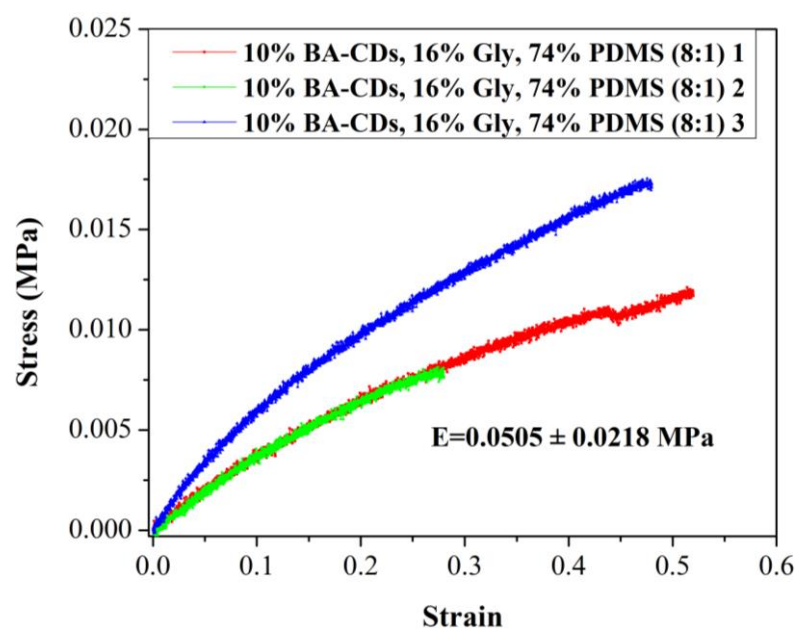


Figure 4.18 Elastic region of the tensile stress-strain curve of triplicate 10% BA-CD, 16% glycerol, and 74% PDMS (8:1) electrodes



Figure 4.19 Triplicate 10% BA-CD, 16% glycerol, and 74% PDMS (8:1) electrodes post-rupture due to applied tensile force

4.3.4 Stability testing: PBS immersion

The best performing electrode composition electrochemically and mechanically was then studied for its stability in an environment similar to the physiological one. Triplicate 10% BA-CD, 16% glycerol, 74% PDMS (8:1) were immersed in 10% PBS for 1 to 12 weeks. EIS and CV were conducted after every 1 week of immersion. The change in size and weight after PBS immersion were also measured to check for any electrode swelling. The EIS and CV data for the electrodes from week 1 until week 7 are shown in Table 4.4. Data obtained from week 8 to 12 are found in the Appendix. There is a notable improvement in impedance at 1 kHz and CSC post-PBS immersion compared to before immersion. This is evident with the large reduction in the impedance at 1 kHz and the increase in CSC post-immersion compared to before PBS immersion. Such improvement in electrochemical properties is expected due to PBS's conductive properties [81]. PBS has a conductivity of 0.014 S/cm [82]. Enhanced electrochemical performance in PBS further adds to the advantages of our electrodes for future implantation purposes since the body's environment is similar to that of PBS. Therefore, we can predict that the electrodes will have a better performance when implanted in the future. This provides a better representation of the electrode performance if implanted in the future.

Although improved performance was observed between PBS immersed and non-immersed electrodes, there was no notable difference in the performance of the electrodes immersed for different periods of time.

Table 4.4 Conductivity, bulk resistance, impedance at 1 kHz, and CSC of the electrodes after PBS immersion for 1 to 7 weeks

Week	R (k Ω)	Impedance at 1 kHz (k Ω)	Conductivity (S/cm)	CSC (μ C/cm ²)
0 (before immersion)	0.795 \pm 0.563	664.45 \pm 297.12	3.087 \pm 3.216 \times 10 ⁻⁴	21.28 \pm 5.816
1	0.187 \pm 0.047	43.73 \pm 27.33	7.4 \pm 2.4 \times 10 ⁻⁴	186.3 \pm 27.8

2	0.216±0.026	100.34±33.51	6.115± 0.83×10 ⁻⁴	204.4± 47.5
3	0.164±0.075	162.08±54.13	9.98± 4.82×10 ⁻⁴	137.8± 36.0
4	0.189±0.012	282.59±153.43	7.00± 0.513×10 ⁻⁴	85.1± 6.0
5	0.114±0.034	154.23±93.61	1.24± 0.353×10 ⁻³	115.1± 33.2
6	0.169±0.048	107.23±96.45	9.81± 5.58×10 ⁻⁴	119.5± 39.9
7	0.096±0.005	53.41±27.31	1.72± 0.0293×10 ⁻³	153.2± 34.0

To evaluate the swelling effect of the electrodes post-PBS immersion, the electrode's weights were recorded before and after implantation. Figure 4.20 shows the changes in weight percentage of the electrode post incubation in PBS for 1 to 7 weeks. The electrodes swelled up until 37.7% of the original weight of the electrode by week 7 of PBS immersion. The observed swelling did not have an effect on the electrode's electrochemical performance as shown in Table 4.4.

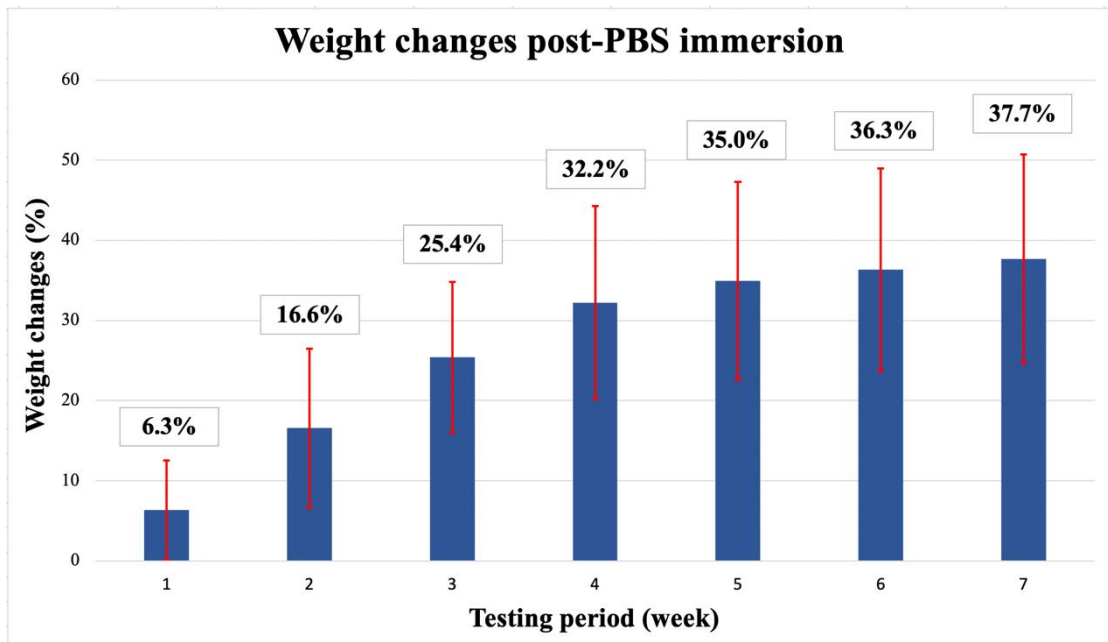


Figure 4.20 Average percentage weight change of triplicate 10% BA-CD, 16% glycerol, and 74% PDMS (8:1) electrodes post-immersion in PBS for 7 weeks

Although the swelling did not affect the electrode performance, it could have negative effects on the electrode when implanted in the future. The increase in volume can cause the electrode to compress the tissues surrounding it at the site of implantation. Furthermore, electrode swelling has been reported to remarkably affect the stability of detected signals and degrade the electrode's mechanical properties [83]. Therefore, future *in vivo* works should ensure the electrodes do not swell to a point that compresses the tissue or disrupts the stability of the signals detected. One possible potential solution worth future investigation is pre-swelling the electrodes before implantation. This could possibly prevent swelling after implantation since the increase in weight seems to start stabilizing at weeks 5 through 7. However, weight change analysis should be conducted over a longer period to confirm that no more swelling is happening after week 7.

Since PDMS is hydrophobic, such swelling of PDMS composites in PBS is not expected. The observed swelling can be explained by the formation of microchannels in PDMS due to the addition of BA-CDs. Additives have been reported to induce the formation of microchannels in PDMS which allow the leaching out of materials and increase the polymer's volume and mass [84]. To examine the formation of microchannels after the addition of BA-CDs, SEM images were obtained for bare PDMS (8:1) and 16% glycerol/84% PDMS (8:1) and compared to that of 10% BA-CD/16% glycerol/74% PDMS (8:1) (Figure 4.6). Figure 4.21 shows the SEM images of bare PDMS and PDMS/glycerol composites. As shown by the SEM images, the PDMS lacked microchannels while PDMS/glycerol had a few microchannels present. This is in comparison to the higher number of microchannels found in the BA-CD- and glycerol-incorporated PDMS (Figure 4.3.3.1). This could explain the swelling observed with the BA-CD/glycerol/PDMS composites incubated in PBS.

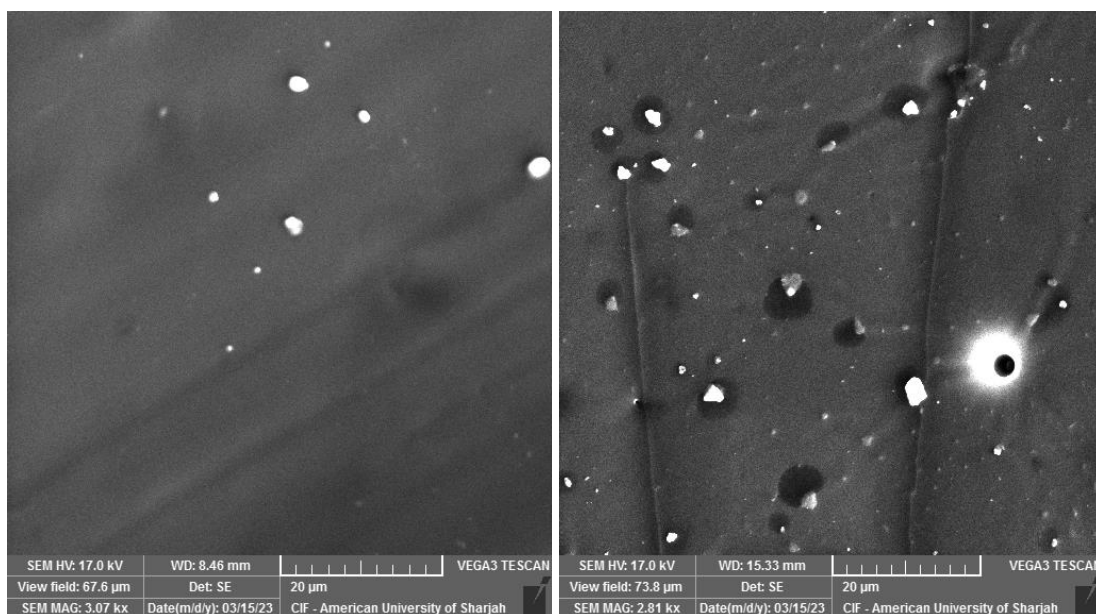


Figure 4.21 SEM images of 100% PDMS 8:1 (left) and 16% glycerol/84% PDMS 8:1 (right)

To ensure the flexibility of the electrode was not reduced due to swelling during PBS incubation, tensile testing was conducted for the electrode after 7 weeks of immersion in PBS. The PBS-incubated 10% BA-CD, 16% glycerol, 74% PDMS (8:1) electrode had an average Young's modulus of 0.1562 ± 0.0274 MPa. PBS incubation reduced the flexibility of the electrodes by increasing the Young's modulus from around 0.0505 MPa to around 0.1562 MPa (more than double). This is mechanically compatible with skin tissue but more rigid than muscle tissue. However, this elasticity is still higher than many other flexible implantable electrodes summarized in Table 4.3. Therefore, PBS immersion negatively influenced elasticity of the electrode composition however to a degree that is still compatible with skin tissue.

4.4 BA-CD/PDMS Electrode Biocompatibility Testing

To evaluate the safety of the composites, MTT (3-(4,5-dimethylthiazol-2-yl)-2,5-diphenyltetrazolium bromide) cytotoxicity assay was conducted with the best performing electrode composed of 10% BA-CD, 16% glycerol, 74% PDMS (8:1). Figure 4.22 shows the cell viability percentage (percentage of alive cells after treatment compared to before treatment) was obtained with bare BA-CDs, bare PDMS (8:1), 16% glycerol/84% PDMS (8:1), and 10% BA-CD/16% glycerol/74% PDMS (8:1) using the MTT assay. The concentration of BA-CDs used was 1 mg/mL, while the other compositions were disks of 1 mm thickness and 1 cm diameter. The cell line used was

HBMEC brain endothelial cells. The cells were exposed to the treatments for 48 hours. While PDMS and PDMS/glycerol were nontoxic to the cells as expected, bare BA-CDs and BA-CD-incorporated electrodes were toxic to the cells reducing their viability to 32.76 and 26%. Based on the ISO 10993 for *in vitro* cytotoxicity assays, a percentage viability lower than 70% indicates the cytotoxic potential of the material being tested. Therefore, currently, the electrodes seem to possess some toxicity toward the cells and this toxicity seems to arise from the BA-CDs. Further studies are needed with other cell lines to have a complete evaluation of cytotoxicity of these electrodes. Since further studies are needed to obtain a more complete idea on the electrode's biocompatibility, their applications can currently be limited to wearable devices.

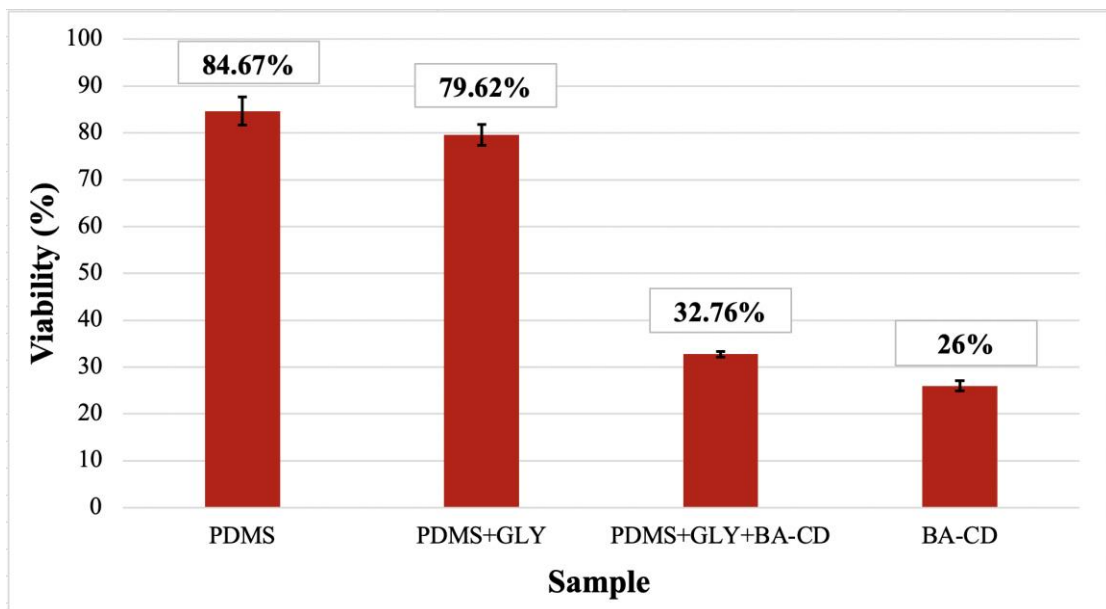


Figure 4.22 Viability of cells exposed to bare BA-CDs, bare PDMS (8:1), 16% glycerol/84% PDMS (8:1), and 10% BA-CD/16% glycerol/74% PDMS (8:1) for 48 hours

4.5 Electrophysiological Signal Recording: ECG and EMG

The ability of the electrodes to record electrophysiological signals was next evaluated using ECG and EMG. Figure 4.23 shows the ECG measured using 10% BA-CD, 16% glycerol, 74% PDMS (8:1) and the commercial Ag/AgCl electrodes with the differential electrodes placed on the wrist and ankle. The results show the electrodes recorded a clean ECG comparable to that recorded with the commercial Ag/AgCl electrodes. Quantitatively, the ECG recorded using 10% BA-CD-doped electrode had a PSNR of 36.75 dB while the Ag/AgCl electrode had a PSNR of 39.98 dB. Therefore, the 10% BA-CD, 16% glycerol, 74% PDMS (8:1) composites recorded a clean ECG

comparable qualitatively and quantitatively to that recorded by the commercial Ag/AgCl electrodes.

To ensure the signal recording ability is due to the incorporation of BA-CDs into the composites, ECG was recorded using 100% PDMS (8:1) and 16% glycerol/84% PDMS (8:1). Readings measured using 100% PDMS (8:1) and 16% glycerol/84% PDMS (8:1) with the differential electrodes placed on the wrist and ankle (shown in the appendix) reveal lack of ability to measure ECG. This indicates the ability to record ECG stems from the incorporation of BA-CDs into the composite.

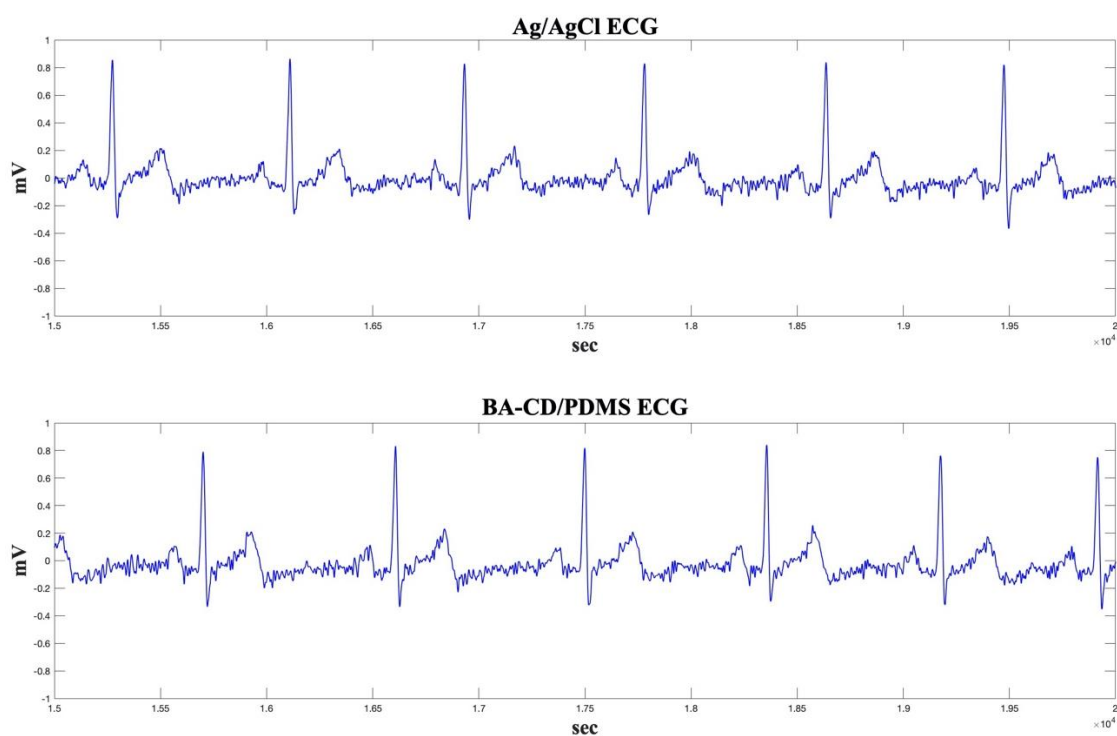


Figure 4.23 ECG measured using 10% BA-CD/16% glycerol/74% PDMS (8:1) and Ag/AgCl electrodes

EMG was next measured using the 10% BA-CD, 16% glycerol, 74% PDMS (8:1) and the commercial Ag/AgCl electrodes. Figure 4.24 shows the EMG measured using the 10% BA-CD, 16% glycerol, 74% PDMS (8:1) and the commercial Ag/AgCl electrodes. The stable regions represent periods of muscle relaxation while the regions of higher amplitudes represent periods of muscle contraction. The BA-CD-doped electrodes recorded ECG with a signal quality comparable to that of the Ag/AgCl electrodes although more noise was recorded with the BA-CD-incorporated electrodes.

To ensure the signal recording ability is due to the incorporation of BA-CDs into the composites, EMG was recorded using 100% PDMS (8:1) and 16% glycerol/84% PDMS (8:1). EMG measured using 100% PDMS (8:1) and 16% glycerol/84% PDMS (8:1) (shown in the appendix) reveal lack of ability of the BA-CD-free composites to measure EMG. This indicates the ability to record EMG stems from the incorporation of BA-CDs into the composite.

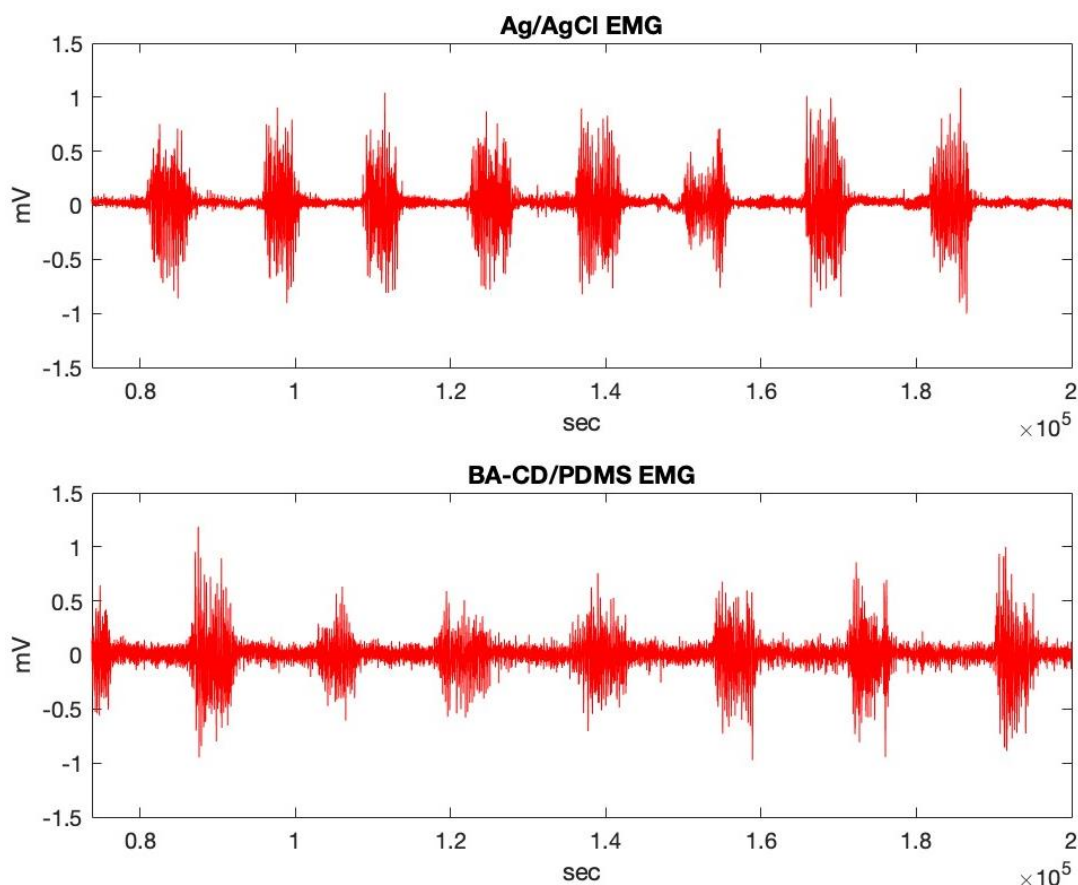


Figure 4.24 EMG measured using 10% BA-CD/16% glycerol/74% PDMS (8:1) and Ag/AgCl electrodes

Overall, the results presented in this chapter indicate the successful synthesis of conductive nano-sized BA-CDs. When incorporated into PDMS, the BA-CDs together with the dispersant glycerol provided conductive electrodes with a flexibility compatible with biological tissues. When incubated in PBS, the electrodes had an improved electrochemical performance due to the conductivity of PBS. The flexibility of the electrodes was reduced post-PBS incubation, however, to a degree still compatible with tissue. Yet, the electrode swelled when immersed in PBS. This could

possibly raise some issues for future implantation. The electrodes also possessed some toxicity towards the cells *in vitro* although more investigation is needed to obtain a complete evaluation of their safety. The electrodes recorded high quality ECG and EMG signals comparable to that of the commercial Ag/AgCl.

Chapter 5. Conclusion and Future work

This thesis reported the synthesis of conductive yet flexible composites to replace the conventional metal-based electrodes for future applications including nerve stimulation, wearable devices, and/or flexible electronics. In this study, the synthesized composites were composed of boronic acid-modified carbon dots (BA-CDs) as the conductive filler and the polymer polydimethylsiloxane (PDMS) as the flexible matrix. The flexible BA-CD/PDMS composites were evaluated for several characteristics that can qualify them as electrodes for neural stimulation or for flexible and wearable electronic applications. The parameters investigated were: 1) electrochemical characteristics (conductivity, bulk impedance, impedance at 1 kHz, and CSC), 2) mechanical: elasticity (Young's modulus), 3) long-term stability, 4) biocompatibility, and 5) surface recording of electrophysiological signals. The composite composition was varied by changing the percentage of BA-CDs and PDMS, incorporating a BA-CD dispersant (glycerol), and varying the curing temperature and PDMS crosslinking density. The effect of each of those variations on the electrode's performance was evaluated to obtain the best performing electrode. Increasing BA-CD percentage with the incorporation of the dispersant glycerol and crosslinking density improved electrode performance. Increasing curing temperature and BA-CD percentage without glycerol, however, negatively influenced the electrode's performance.

The best performing electrode was composed of 10% BA-CDs, 16% glycerol, and 74% PDMS crosslinked with an 8:1 elastomer:curing agent ratio. Mechanically, the electrodes had an elasticity comparable to the biological tissues. In phosphate buffer saline, a body-like environment, the 10% BA-CDs, 16% glycerol, and 74% PDMS (8:1) electrodes had improved electrochemical performance although their elasticity was reduced. However, their elasticity was still compatible with biological tissues. In terms of toxicity, the electrodes showed relatively high toxicity towards brain cells *in vitro*. However, triplicate assays are needed to have a complete evaluation of those results. In terms of recording electrophysiological signals, the electrodes recorded ECG and EMG with a signal quality comparable to that of the commercial Ag/AgCl electrodes.

Therefore, the electrodes developed in this work based on BA-CDs and PDMS were conductive with low impedance, elastic to a degree compatible with biological tissues, capable of withstanding weeks of incubation in PBS while maintaining their

structural integrity, electrochemical performance, and elasticity, and capable of recording high quality ECG and EMG signals as surface electrodes. However, it is worth noting that the electrodes experienced swelling post-incubation in PBS. This could present a drawback that needs to be addressed in future *in vivo* works.

To further progress with this work, further biocompatibility testing should be conducted. Preferably, those studies should be conducted on the conventional fibroblast L929 cells used for biocompatibility testing of biomaterials. More importantly, a dose response experiment must be conducted where the cells are treated with different dosages of the electrode material. This is important to determine dose above which the material is toxic to the cells. The toxicity could be reduced by restricting the electrode material below a specific dose. This is because the material could present dose-dependent toxicity to the cells and the composite could be safe to the cells if maintained below a specific threshold concentration.

References

- [1] R. B. Campenot, *Animal electricity: how we learned that the body and brain are electric machines*. Cambridge, Massachusetts: Harvard University Press, 2016.
- [2] D. S. Faber and A. E. Pereda, “Two Forms of Electrical Transmission Between Neurons,” *Front. Mol. Neurosci.*, vol. 11, p. 427, Nov. 2018, doi: 10.3389/fnmol.2018.00427.
- [3] A. Waugh and A. Grant, “Anatomy and Physiology in Health and Illness,” *Ross and Wilson*, p. 495, 2001.
- [4] B. Lopes *et al.*, “Peripheral Nerve Injury Treatments and Advances: One Health Perspective,” *IJMS*, vol. 23, no. 2, p. 918, Jan. 2022, doi: 10.3390/ijms23020918.
- [5] Y. Shi, R. Liu, L. He, H. Feng, Y. Li, and Z. Li, “Recent development of implantable and flexible nerve electrodes,” *Smart Materials in Medicine*, vol. 1, pp. 131–147, 2020, doi: 10.1016/j.smaim.2020.08.002.
- [6] W. Yang, Y. Gong, and W. Li, “A Review: Electrode and Packaging Materials for Neurophysiology Recording Implants,” *Front. Bioeng. Biotechnol.*, vol. 8, p. 622923, Jan. 2021, doi: 10.3389/fbioe.2020.622923.
- [7] E. A. Cuttaz, C. A. R. Chapman, O. Syed, J. A. Goding, and R. A. Green, “Stretchable, Fully Polymeric Electrode Arrays for Peripheral Nerve Stimulation,” *Adv. Sci.*, vol. 8, no. 8, p. 2004033, Apr. 2021, doi: 10.1002/advs.202004033.
- [8] Y. Long, J. Li, F. Yang, J. Wang, and X. Wang, “Wearable and Implantable Electroceuticals for Therapeutic Electrostimulations,” *Adv. Sci.*, vol. 8, no. 8, p. 2004023, Apr. 2021, doi: 10.1002/advs.202004023.
- [9] A. Ersen and M. Sahin, “Polydimethylsiloxane-based optical waveguides for tetherless powering of floating microstimulators,” *J. Biomed. Opt.*, vol. 22, no. 5, p. 055005, May 2017, doi: 10.1117/1.JBO.22.5.055005.
- [10] C. Hassler, T. Boretius, and T. Stieglitz, “Polymers for neural implants,” *J. Polym. Sci. B Polym. Phys.*, vol. 49, no. 1, pp. 18–33, Jan. 2011, doi: 10.1002/polb.22169.
- [11] J.-Y. Baek, J.-H. An, J.-M. Choi, K.-S. Park, and S.-H. Lee, “Flexible polymeric dry electrodes for the long-term monitoring of ECG,” *Sensors and Actuators A: Physical*, vol. 143, no. 2, pp. 423–429, May 2008, doi: 10.1016/j.sna.2007.11.019.

- [12] W. R. Lee, C. Im, H.-Y. Park, J.-M. Seo, and J.-M. Kim, "Fabrication of Convex PDMS–Parylene Microstructures for Conformal Contact of Planar Micro-Electrode Array," *Polymers*, vol. 11, no. 9, p. 1436, Sep. 2019, doi: 10.3390/polym11091436.
- [13] G.-H. Kwon *et al.*, "Fabrication and Evaluation of the Flexible and Implantable Soft Micro Electrode for Retinal Prosthesis," *IEEE*, p. 3, doi: 10.1109/BMN.2006.330934.
- [14] Y. Chen *et al.*, "Effect of Microgroove Structure in PDMS-Based Silicone Implants on Biocompatibility," *Front. Bioeng. Biotechnol.*, vol. 9, p. 793778, Jan. 2022, doi: 10.3389/fbioe.2021.793778.
- [15] H. Zhao, R. Liu, H. Zhang, P. Cao, Z. Liu, and Y. Li, "Research Progress on the Flexibility of an Implantable Neural Microelectrode," *Micromachines*, vol. 13, no. 3, p. 386, Feb. 2022, doi: 10.3390/mi13030386.
- [16] P. Du, X. Lin, and X. Zhang, "Characterization on the Electrical Properties of PDMS Nanocomposites by Conducting Polymer Nanowires," *MRS Proc.*, vol. 1312, pp. mrsf10-1312-ii03-15, 2011, doi: 10.1557/opl.2011.110.
- [17] J. H. Kim *et al.*, "Simple and cost-effective method of highly conductive and elastic carbon nanotube/polydimethylsiloxane composite for wearable electronics," *Sci Rep*, vol. 8, no. 1, p. 1375, Dec. 2018, doi: 10.1038/s41598-017-18209-w.
- [18] A. Al-Othman, S. El-Sadek, C. Momah, M. NARAYANAN, and H. Al-NASHASH, "Synthesis and Characterization of Flexible Implantable Electrodes Using Conductive Polymers," *11TH INTERNATIONAL CONFERENCE ON COMPOSITE SCIENCE AND TECHNOLOGY*, p. 8.
- [19] A. Alatoom, A. Al-Othman, H. Al-Nashash, and M. Al-Sayah, "Development and Characterization of Novel Composite and Flexible Electrode Based on Titanium Dioxide," *IEEE Trans. Compon., Packag. Manufact. Technol.*, vol. 10, no. 7, pp. 1079–1087, Jul. 2020, doi: 10.1109/TCPMT.2020.3001812.
- [20] M. Hamzeh and G. I. Sunahara, "In vitro cytotoxicity and genotoxicity studies of titanium dioxide (TiO₂) nanoparticles in Chinese hamster lung fibroblast cells," *Toxicol in Vitro*, vol. 27, no. 2, pp. 864–873, Mar. 2013, doi: 10.1016/j.tiv.2012.12.018.
- [21] N. Almufleh, A. Al-Othman, Z. Alani, M. H. Al-Sayah, and H. Al-Nashash, "Highly Flexible Polyaniline-Based Implantable Electrode Materials for Neural Sensing/Stimulation Applications," *Electronic Materials*, vol. 2, no. 3, pp. 413–427, Sep. 2021, doi: 10.3390/electronicmat2030028.

- [22] P. Humpolicek, V. Kasparikova, P. Saha, and J. Stejskal, “Biocompatibility of polyaniline,” *Synthetic Metals*, vol. 162, no. 7–8, pp. 722–727, May 2012, doi: 10.1016/j.synthmet.2012.02.024.
- [23] L. Gerrits, R. Hammink, and P. H. J. Kouwer, “Semiflexible polymer scaffolds: an overview of conjugation strategies,” *Polym. Chem.*, vol. 12, no. 10, pp. 1362–1392, 2021, doi: 10.1039/D0PY01662D.
- [24] B. D. Mansuriya and Z. Altintas, “Carbon Dots: Classification, Properties, Synthesis, Characterization, and Applications in Health Care—An Updated Review (2018–2021),” *Nanomaterials*, vol. 11, no. 10, p. 2525, Sep. 2021, doi: 10.3390/nano11102525.
- [25] N. Satō, *Electrochemistry at metal and semiconductor electrodes*. Amsterdam ; New York: Elsevier, 1998.
- [26] N. L. Strominger, R. J. Demarest, and L. B. Laemle, *Noback’s Human Nervous System, Seventh Edition*. Totowa, NJ: Humana Press, 2012. doi: 10.1007/978-1-61779-779-8.
- [27] P. Rea, *Essential clinical anatomy of the nervous system*. Amsterdam ; Boston: Elsevier/AP, Academic Press is an imprint of Elsevier, 2015.
- [28] B. Radić, “Peripheral Nerve Injury in Sports,” *ACC*, 2018, doi: 10.20471/acc.2018.57.03.20.
- [29] M. McAvoy *et al.*, “Flexible Multielectrode Array for Skeletal Muscle Conditioning, Acetylcholine Receptor Stabilization and Epimysial Recording After Critical Peripheral Nerve Injury,” *Theranostics*, vol. 9, no. 23, pp. 7099–7107, 2019, doi: 10.7150/thno.35436.
- [30] H.-C. Tian *et al.*, “Enhanced Flexible Tubular Microelectrode with Conducting Polymer for Multi-Functional Implantable Tissue-Machine Interface,” *Sci Rep*, vol. 6, no. 1, p. 26910, Jun. 2016, doi: 10.1038/srep26910.
- [31] P. H. Peckham, D. M. Ackermann, and C. W. Moss, “The Role of Biomaterials in Stimulating Bioelectrodes,” in *Biomaterials Science*, Elsevier, 2013, pp. 981–996. doi: 10.1016/B978-0-08-087780-8.00084-X.
- [32] J. Jeong, N. Chou, and S. Kim, “Long-term characterization of neural electrodes based on parylene-caulked polydimethylsiloxane substrate,” *Biomed Microdevices*, vol. 18, no. 3, p. 42, Jun. 2016, doi: 10.1007/s10544-016-0065-z.

- [33] D. N. Heo *et al.*, “Flexible and Highly Biocompatible Nanofiber-Based Electrodes for Neural Surface Interfacing,” *ACS Nano*, vol. 11, no. 3, pp. 2961–2971, Mar. 2017, doi: 10.1021/acsnano.6b08390.
- [34] X. S. Zheng *et al.*, “Evaluation of a conducting elastomeric composite material for intramuscular electrode application,” *Acta Biomaterialia*, vol. 103, pp. 81–91, Feb. 2020, doi: 10.1016/j.actbio.2019.12.021.
- [35] J. Qu, L. Ouyang, C. Kuo, and D. C. Martin, “Stiffness, strength and adhesion characterization of electrochemically deposited conjugated polymer films,” *Acta Biomaterialia*, vol. 31, pp. 114–121, Feb. 2016, doi: 10.1016/j.actbio.2015.11.018.
- [36] V. Sankar *et al.*, “A Highly Compliant Serpentine Shaped Polyimide Interconnect for Front-End Strain Relief in Chronic Neural Implants,” *Front. Neurol.*, vol. 4, 2013, doi: 10.3389/fneur.2013.00124.
- [37] M. A. McClain, I. P. Clements, R. H. Shafer, R. V. Bellamkonda, M. C. LaPlaca, and M. G. Allen, “Highly-compliant, microcable neuroelectrodes fabricated from thin-film gold and PDMS,” *Biomed Microdevices*, vol. 13, no. 2, pp. 361–373, Apr. 2011, doi: 10.1007/s10544-010-9505-3.
- [38] M. S. Heo, H. S. Moon, H. C. Kim, H. W. Park, Y. H. Lim, and S. H. Paek, “Fully Implantable Deep Brain Stimulation System with Wireless Power Transmission for Long-term Use in Rodent Models of Parkinson’s Disease,” *J Korean Neurosurg Soc*, vol. 57, no. 3, p. 152, 2015, doi: 10.3340/jkns.2015.57.3.152.
- [39] M. N. Barshutina *et al.*, “PDMS-CNT composite for soft bioelectronic neuronal implants,” *Composites Part B: Engineering*, vol. 247, p. 110286, Dec. 2022, doi: 10.1016/j.compositesb.2022.110286.
- [40] K. Xu *et al.*, “Effect of Electrical and Electromechanical Stimulation on PC12 Cell Proliferation and Axon Outgrowth,” *Front. Bioeng. Biotechnol.*, vol. 9, p. 757906, Oct. 2021, doi: 10.3389/fbioe.2021.757906.
- [41] C. L. Kolarcik *et al.*, “Elastomeric and soft conducting microwires for implantable neural interfaces,” *Soft Matter*, vol. 11, no. 24, pp. 4847–4861, 2015, doi: 10.1039/C5SM00174A.
- [42] L. M. Ferrari *et al.*, “All-Polymer Printed Low-Cost Regenerative Nerve Cuff Electrodes,” *Front. Bioeng. Biotechnol.*, vol. 9, p. 615218, Feb. 2021, doi: 10.3389/fbioe.2021.615218.

- [43] A. A. Guex, N. Vachicouras, A. E. Hight, M. C. Brown, D. J. Lee, and S. P. Lacour, "Conducting polymer electrodes for auditory brainstem implants," *J. Mater. Chem. B*, vol. 3, no. 25, pp. 5021–5027, 2015, doi: 10.1039/C5TB00099H.
- [44] G. Nocito *et al.*, "Carbon Dots as Promising Tools for Cancer Diagnosis and Therapy," *Cancers*, vol. 13, no. 9, p. 1991, Apr. 2021, doi: 10.3390/cancers13091991.
- [45] J. Liu, R. Li, and B. Yang, "Carbon Dots: A New Type of Carbon-Based Nanomaterial with Wide Applications," *ACS Cent. Sci.*, vol. 6, no. 12, pp. 2179–2195, Dec. 2020, doi: 10.1021/acscentsci.0c01306.
- [46] K. O. Boakye-Yiadom *et al.*, "Carbon dots: Applications in bioimaging and theranostics," *Int. J. Pharm.*, vol. 564, pp. 308–317, Jun. 2019, doi: 10.1016/j.ijpharm.2019.04.055.
- [47] S.-T. Yang *et al.*, "Carbon Dots for Optical Imaging in Vivo," *J. Am. Chem. Soc.*, vol. 131, no. 32, pp. 11308–11309, Aug. 2009, doi: 10.1021/ja904843x.
- [48] Q. Wang *et al.*, "Nonblinking carbon dots for imaging and tracking receptors on a live cell membrane," *Chem. Commun.*, vol. 57, no. 45, pp. 5554–5557, 2021, doi: 10.1039/D1CC01120K.
- [49] T. Feng and Y. Zhao, "Preparation of Responsive Carbon Dots for Anticancer Drug Delivery," in *Pharmaceutical Nanotechnology*, V. Weissig and T. Elbayoumi, Eds., in *Methods in Molecular Biology*, vol. 2000. New York, NY: Springer New York, 2019, pp. 227–234. doi: 10.1007/978-1-4939-9516-5_15.
- [50] S. Campuzano, P. Yáñez-Sedeño, and J. M. Pingarrón, "Carbon Dots and Graphene Quantum Dots in Electrochemical Biosensing," *Nanomaterials*, vol. 9, no. 4, p. 634, Apr. 2019, doi: 10.3390/nano9040634.
- [51] S. S. Shankar, R. M. Shereema, V. Ramachandran, T. V. Sruthi, V. B. S. Kumar, and R. B. Rakhi, "Carbon Quantum Dot-Modified Carbon Paste Electrode-Based Sensor for Selective and Sensitive Determination of Adrenaline," *ACS Omega*, vol. 4, no. 4, pp. 7903–7910, Apr. 2019, doi: 10.1021/acsomega.9b00230.
- [52] J. T. Nivaldo, *Introductory chemistry essentials*, Fifth. Fifth. Pearson, 2017.
- [53] K. Borzutzki and G. Brunklaus, "Carriers of the Spatial Distribution of Charge Magnetic Resonance Imaging Studies," p. 32.

- [54] P. Das *et al.*, “Biocompatible carbon dots derived from κ -carrageenan and phenyl boronic acid for dual modality sensing platform of sugar and its anti-diabetic drug release behavior,” *International Journal of Biological Macromolecules*, vol. 132, pp. 316–329, Jul. 2019, doi: 10.1016/j.ijbiomac.2019.03.224.
- [55] S. Kiran and R. D. K. Misra, “Mechanism of intracellular detection of glucose through nonenzymatic and boronic acid functionalized carbon dots,” *J. Biomed. Mater. Res.*, vol. 103, no. 9, pp. 2888–2897, Sep. 2015, doi: 10.1002/jbm.a.35421.
- [56] P. Shen and Y. Xia, “Synthesis-Modification Integration: One-Step Fabrication of Boronic Acid Functionalized Carbon Dots for Fluorescent Blood Sugar Sensing,” *Anal. Chem.*, vol. 86, no. 11, pp. 5323–5329, Jun. 2014, doi: 10.1021/ac5001338.
- [57] S. Xu *et al.*, “One-step fabrication of boronic-acid-functionalized carbon dots for the detection of sialic acid,” *Talanta*, vol. 197, pp. 548–552, May 2019, doi: 10.1016/j.talanta.2019.01.074.
- [58] D. E. Albert, “Methods for Verifying Medical Device Cleanliness,” in *Developments in Surface Contamination and Cleaning*, Elsevier, 2015, pp. 109–128. doi: 10.1016/B978-0-323-31303-2.00004-2.
- [59] D. A. Skoog, F. J. Holler, and S. R. Crouch, *Principles of instrumental analysis*, 6th ed. Belmont, CA: Thomson Brooks/Cole, 2007.
- [60] D. Koga, S. Kusumi, M. Shibata, and T. Watanabe, “Applications of Scanning Electron Microscopy Using Secondary and Backscattered Electron Signals in Neural Structure,” *Front. Neuroanat.*, vol. 15, p. 759804, Dec. 2021, doi: 10.3389/fnana.2021.759804.
- [61] F. A. Shah, K. Ruscsák, and A. Palmquist, “50 years of scanning electron microscopy of bone—a comprehensive overview of the important discoveries made and insights gained into bone material properties in health, disease, and taphonomy,” *Bone Res*, vol. 7, no. 1, p. 15, May 2019, doi: 10.1038/s41413-019-0053-z.
- [62] H. S. Magar, R. Y. A. Hassan, and A. Mulchandani, “Electrochemical Impedance Spectroscopy (EIS): Principles, Construction, and Biosensing Applications,” *Sensors*, vol. 21, no. 19, p. 6578, Oct. 2021, doi: 10.3390/s21196578.
- [63] A. R. Harris, C. Newbold, D. Stathopoulos, P. Carter, R. Cowan, and G. G. Wallace, “Comparison of the In Vitro and In Vivo Electrochemical Performance of Bionic Electrodes,” *Micromachines*, vol. 13, no. 1, p. 103, Jan. 2022, doi: 10.3390/mi13010103.

- [64] N. Elgrishi, K. J. Rountree, B. D. McCarthy, E. S. Rountree, T. T. Eisenhart, and J. L. Dempsey, "A Practical Beginner's Guide to Cyclic Voltammetry," *J. Chem. Educ.*, vol. 95, no. 2, pp. 197–206, Feb. 2018, doi: 10.1021/acs.jchemed.7b00361.
- [65] N. Özkaya, D. Leger, D. Goldsheyder, and M. Nordin, *Fundamentals of Biomechanics: Equilibrium, Motion, and Deformation*. Cham: Springer International Publishing, 2017. doi: 10.1007/978-3-319-44738-4.
- [66] M. M. R. Howlader, T. E. Doyle, S. Mohtashami, and J. R. Kish, "Charge transfer and stability of implantable electrodes on flexible substrate," *Sens. Actuators B Chem.*, vol. 178, pp. 132–139, Mar. 2013, doi: 10.1016/j.snb.2012.12.051.
- [67] C. Pélabon, C. H. Hilde, S. Einum, and M. Gamelon, "On the use of the coefficient of variation to quantify and compare trait variation," *Evolution Letters*, vol. 4, no. 3, pp. 180–188, Jun. 2020, doi: 10.1002/evl3.171.
- [68] R. Ospina and F. Marmolejo-Ramos, "Performance of Some Estimators of Relative Variability," *Front. Appl. Math. Stat.*, vol. 5, p. 43, Aug. 2019, doi: 10.3389/fams.2019.00043.
- [69] N. H. Nam and N. H. Luong, "Nanoparticles: synthesis and applications," in *Materials for Biomedical Engineering*, Elsevier, 2019, pp. 211–240. doi: 10.1016/B978-0-08-102814-8.00008-1.
- [70] M. Z. Fahmi *et al.*, "Design of boronic acid-attributed carbon dots on inhibits HIV-1 entry," *RSC Adv.*, vol. 6, no. 95, pp. 92996–93002, 2016, doi: 10.1039/C6RA21062G.
- [71] Y. Zare, "Study of nanoparticles aggregation/agglomeration in polymer particulate nanocomposites by mechanical properties," *Composites Part A: Applied Science and Manufacturing*, vol. 84, pp. 158–164, May 2016, doi: 10.1016/j.compositesa.2016.01.020.
- [72] S. Tamayo-Vegas, A. Muhsan, C. Liu, M. Tarfaoui, and K. Lafdi, "The Effect of Agglomeration on the Electrical and Mechanical Properties of Polymer Matrix Nanocomposites Reinforced with Carbon Nanotubes," *Polymers*, vol. 14, no. 9, p. 1842, Apr. 2022, doi: 10.3390/polym14091842.
- [73] A. Al-Othman, A. Y. Tremblay, W. Pell, Y. Liu, B. A. Peppley, and M. Ternan, "The effect of glycerol on the conductivity of Nafion-free ZrP/PTFE composite membrane electrolytes for direct hydrocarbon fuel cells," *J. Power Sources*, vol. 199, pp. 14–21, Feb. 2012, doi: 10.1016/j.jpowsour.2011.09.104.

[74] H. Suherman, A. B. Sulong, and J. Sahari, "Effect of Filler Loading Concentration, Curing Temperature and Molding Pressure on The Electrical Conductivity of CNTs/Graphite/Epoxy Nanocomposites at High Loading of Conductive Fillers".

[75] K. Berean *et al.*, "The effect of crosslinking temperature on the permeability of PDMS membranes: Evidence of extraordinary CO₂ and CH₄ gas permeation," *Separation and Purification Technology*, vol. 122, pp. 96–104, Feb. 2014, doi: 10.1016/j.seppur.2013.11.006.

[76] C. Jin, C. Ma, Z. Yang, and H. Lin, "A Force Measurement Method Based on Flexible PDMS Grating," *Applied Sciences*, vol. 10, no. 7, p. 2296, Mar. 2020, doi: 10.3390/app10072296.

[77] J. Zhao, P. Yu, and S. Dong, "The Influence of Crosslink Density on the Failure Behavior in Amorphous Polymers by Molecular Dynamics Simulations," *Materials*, vol. 9, no. 4, p. 234, Mar. 2016, doi: 10.3390/ma9040234.

[78] O. Mohamed, A. Al-Othman, H. Al-Nashash, M. Tawalbeh, F. Almomani, and M. Rezakazemi, "Fabrication of titanium dioxide nanomaterial for implantable highly flexible composite bioelectrode for biosensing applications," *Chemosphere*, vol. 273, p. 129680, Jun. 2021, doi: 10.1016/j.chemosphere.2021.129680.

[79] I. V. Ogneva, D. V. Lebedev, and B. S. Shenkman, "Transversal Stiffness and Young's Modulus of Single Fibers from Rat Soleus Muscle Probed by Atomic Force Microscopy," *Biophysical Journal*, vol. 98, no. 3, pp. 418–424, Feb. 2010, doi: 10.1016/j.bpj.2009.10.028.

[80] M. F. Griffin, B. C. Leung, Y. Premakumar, M. Szarko, and P. E. Butler, "Comparison of the mechanical properties of different skin sites for auricular and nasal reconstruction," *J of Otolaryngol - Head & Neck Surg*, vol. 46, no. 1, p. 33, Dec. 2017, doi: 10.1186/s40463-017-0210-6.

[81] S. De Faveri *et al.*, "Bio-inspired hybrid microelectrodes: a hybrid solution to improve long-term performance of chronic intracortical implants," *Front. Neuroeng.*, vol. 7, Apr. 2014, doi: 10.3389/fneng.2014.00007.

[82] A. Salmanzadeh, M. B. Sano, R. C. Gallo-Villanueva, P. C. Roberts, E. M. Schmelz, and R. V. Davalos, "Investigating dielectric properties of different stages of syngeneic murine ovarian cancer cells," *Biomicrofluidics*, vol. 7, no. 1, p. 011809, Jan. 2013, doi: 10.1063/1.4788921.

[83] X. Xia *et al.*, “Intrinsically Electron Conductive, Antibacterial, and Anti-swelling Hydrogels as Implantable Sensors for Bioelectronics,” *Adv Funct Materials*, vol. 32, no. 48, p. 2208024, Nov. 2022, doi: 10.1002/adfm.202208024.

[84] B. Mikolaszek, J. Kazlauske, A. Larsson, and M. Sznitowska, “Controlled Drug Release by the Pore Structure in Polydimethylsiloxane Transdermal Patches,” *Polymers*, vol. 12, no. 7, p. 1520, Jul. 2020, doi: 10.3390/polym12071520.

Appendix A

ECG: controls

PDMS and PDMS/glycerol electrodes were used as controls to measure ECG. This step is performed to ensure that the ability to record ECG was due to the presence of the conductive BA-CDs and that PDMS and PDMS/glycerol do not inherently possess the ability to record ECG. Recordings obtained using PDMS and PDMS/glycerol are shown in Figure i PDMS shows a completely random noisy signal and clearly fails to pick up any ECG signals. This is expected due to its lack of conductivity. PDMS/glycerol, on the other hand, shows a signal that at first seems to represent that of an ECG. However, zooming in onto the signal recorded with the PDMS/glycerol electrodes indicates the ECG signal lacks the definite shape of the QRS ECG region. Therefore, the signal obtained with the PDMS/Glycerol is distorted due to the noise and interference overriding the signal and does not represent that of an ECG. This is expected due to the relatively poor conductivity of PDMS/Glycerol electrodes. Figure ii shows the zoomed in portions of the readings obtained with Ag/AgCl, BA-CD/PDMS/Glycerol, and PDMS/Glycerol electrodes.

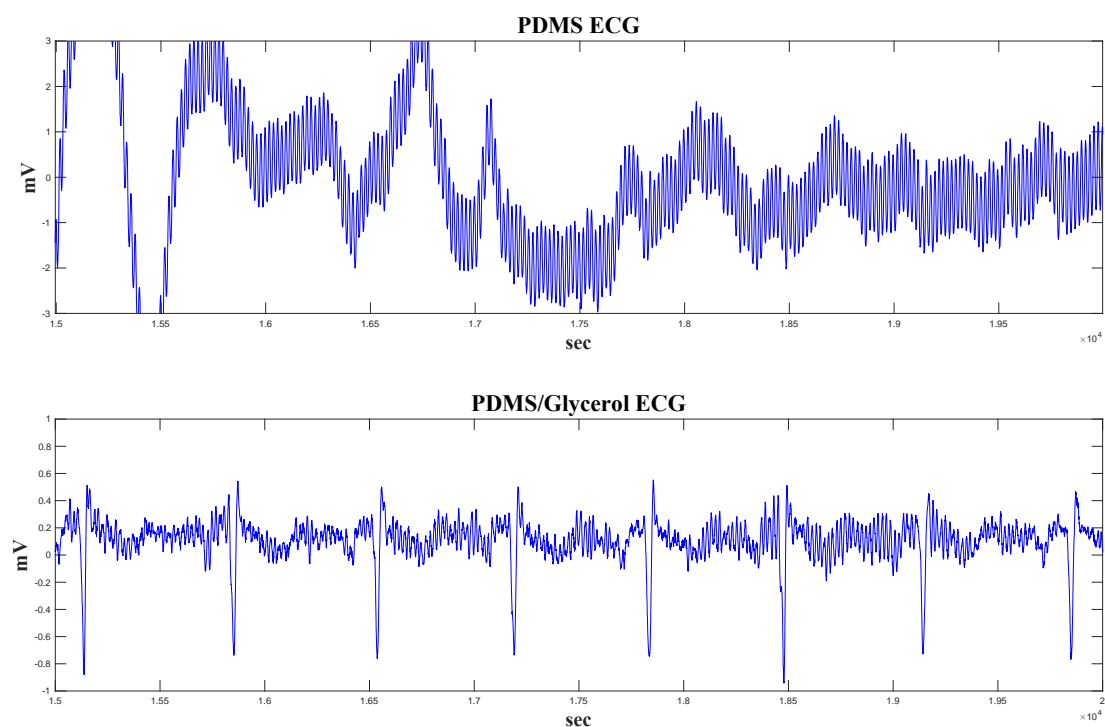


Figure A.1 ECG recording using bare PDMS and PDMS/glycerol when the composite attached to the positive terminal is placed on the left ankle.

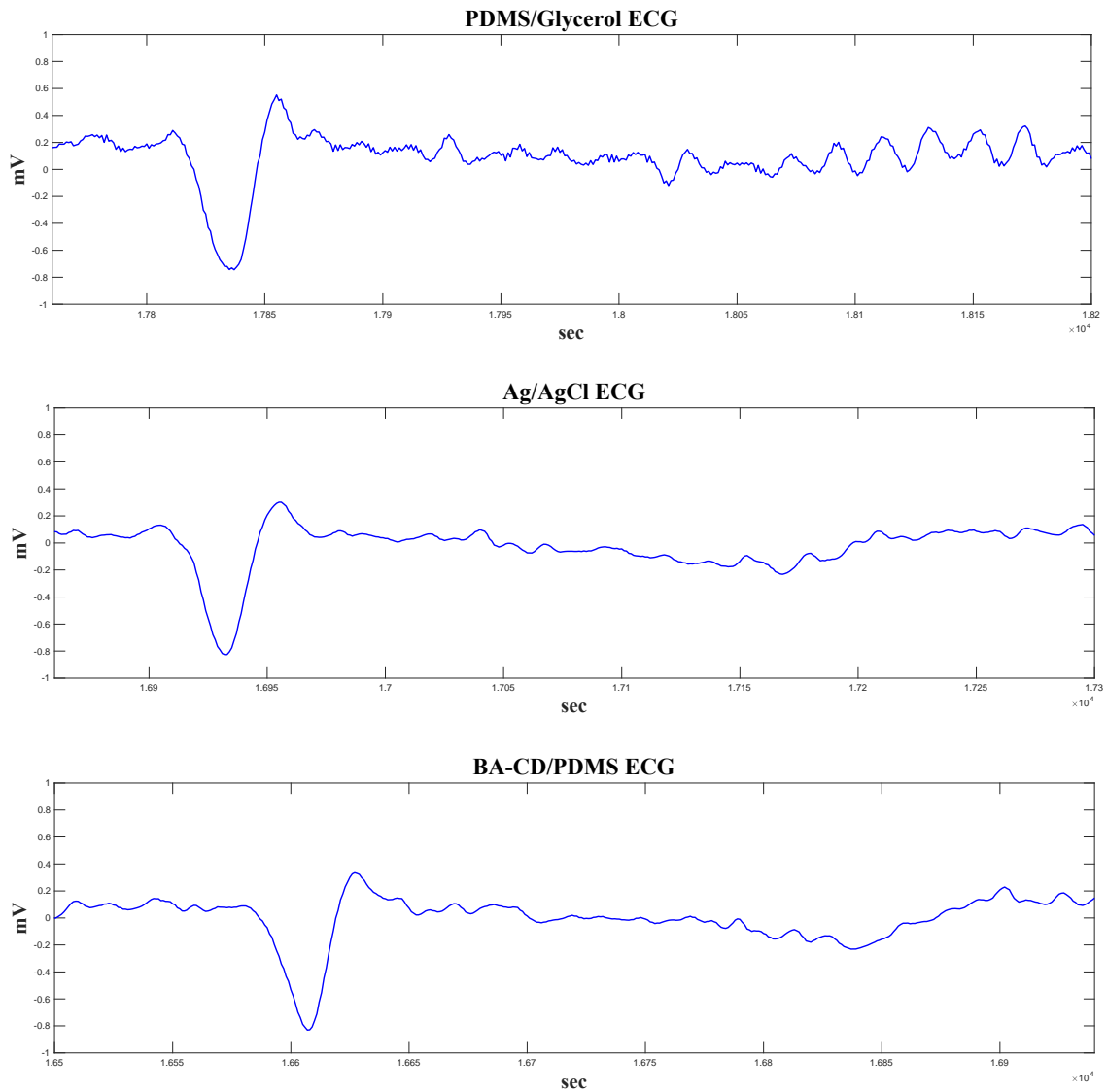


Figure A.2 Zoomed in portions of the readings obtained with PDMS/Glycerol, Ag/AgCl, and BA-CD/PDMS/Glycerol. High frequency noise is overriding the PDMS/Glycerol signal but lacking in the Ag/AgCl and BA-CD/PDMS/Glycerol ECG

EMG: controls

To ensure the ability to measure EMG was due to the presence of BA-CDs and that the bare PDMS and PDMS/glycerol do not inherently possess the ability to record EMG, muscle activity was recorded with PDMS and PDMS/glycerol as shown in

Figure iii. PDMS and PDMS/glycerol both failed to measure muscle activity indicating that the ability to record EMG is due to the presence of BA-CDs.

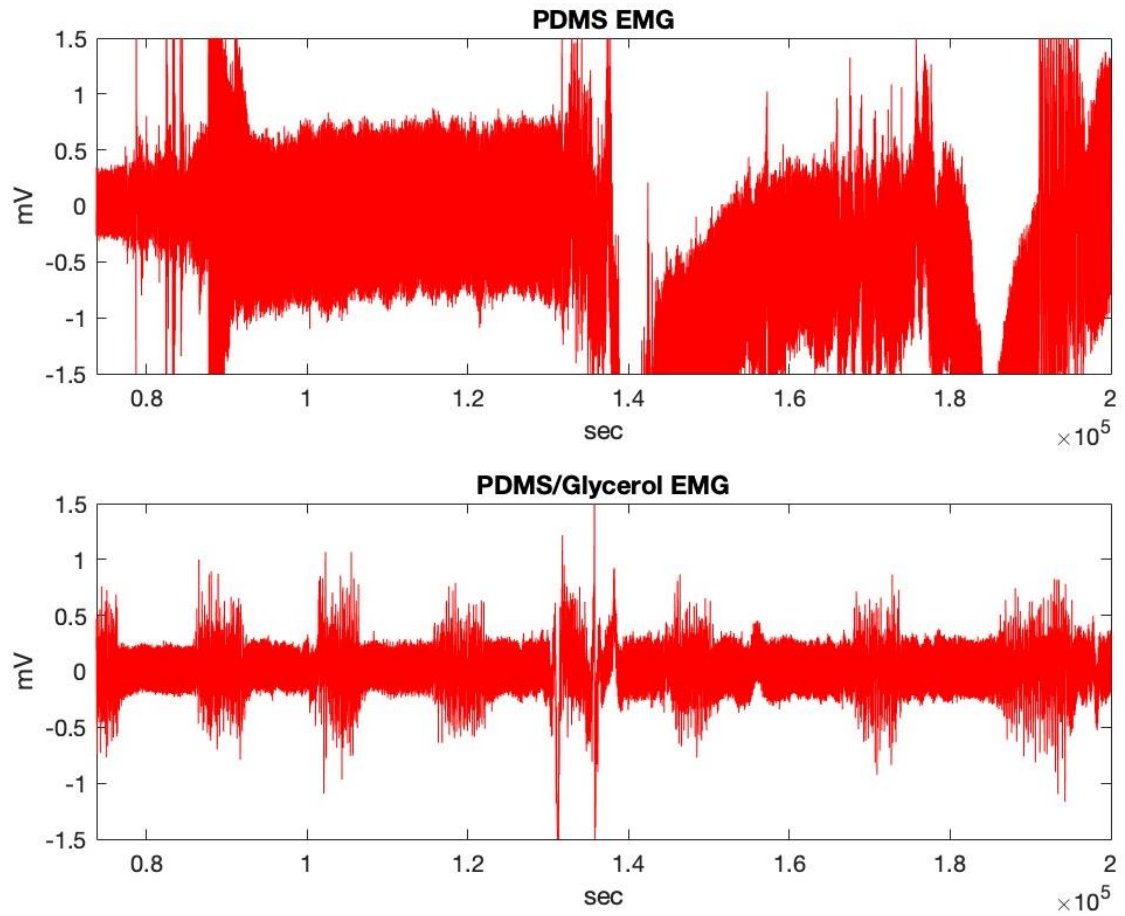


Figure A.3 EMG recording using PDMS and PDMS/glycerol

Stability Testing: weeks 8 to 12

Table A.1 Conductivity, bulk resistance, impedance at 1 kHz, and CSC of the electrodes after PBS immersion for 8 to 12 weeks

Week	R (k Ω)	Impedance at 1 kHz (k Ω)	Conductivity (S/cm)	CSC (μ C/cm ²)
8	0.170 \pm 0.040	126.36 \pm 114.7	7.80 \pm 1.72 \times 10 ⁻⁴	89.6 \pm 20.5
9	0.137 \pm 0.042	269.09 \pm 209.17	9.95 \pm 2.49 \times 10 ⁻⁴	89.9 \pm 17.1

10	0.146±0.040	115.69±19.98	9.26± 2.74×10 ⁻⁴	68.9± 5.9
11	0.154±0.059	457.06±306.77	9.42± 4.06×10 ⁻⁴	53.8± 21.2
12	0.170±0.039	126.36±114.69	7.80± 1.72×10 ⁻⁴	83.8± 42.0

Vita

Amaal Abdulraheb Ali was born in Riyadh, Kingdom of Saudi Arabia (KSA). She received her primary and secondary education in Riyadh, KSA. She received her B.Sc. degree in Life Sciences from the Alfaisal University, Riyadh, KSA in 2020.

In September 2021, she joined the Biomedical Engineering master's program in the American University of Sharjah as a graduate research assistant. During her master's study, she was the co-author of 2 high impact factor review papers and 3 conferences papers which were presented in national and international (US) IEEE conferences. She was also awarded the “Excellence in Research” award and a 10,000 AED grant for her work on implantable electrodes. Her research interests are in nano-biomaterials and nanomedicine.